Shortened lifespan induced by a high-glucose diet is associated with intestinal immune dysfunction in *Drosophila sechellia*

Running title

Effects of high-glucose diet on fruit flies

Maiko Abe[1], Takumi Kamiyama[2], Yasushi Izumi[3,4], Qingyin Qian[5], Yuma Yoshihashi[6], Yousuke Degawa[6], Kaori Watanabe[7], Yukako Hattori[7], Tadashi Uemura[7,8,9], and Ryusuke Niwa[2,9,*]

[1] Degree Programs in Life and Earth Sciences, Graduate School of Science and Technology, University of Tsukuba, Tennodai 1-1-1, Tsukuba, Ibaraki 305-8572, Japan

[2] Life Science Center for Survival Dynamics, Tsukuba Advanced Research Alliance (TARA), University of Tsukuba, Tennodai 1-1-1, Tsukuba, Ibaraki 305-8577, Japan

[3] Division of Cell Structure, National Institute for Physiological Sciences, Okazaki, Aichi 444-8787, Japan.

[4] Department of Physiological Sciences, School of Life Science, SOKENDAI (Graduate University for Advanced Studies), Okazaki, Aichi 444-8585, Japan.

[5] Ph.D. Program in Human Biology, School of Integrative and Global Majors, University of Tsukuba, Tennodai 1-1-1, Tsukuba, Ibaraki 305-8577, Japan

[6] Sugadaira Research Station, Mountain Science Center, University of Tsukuba, Sugadairakogen 1278-294, Nagano 386-2204, Japan

[7] Graduate School of Biostudies, Kyoto University, Kyoto 606-8501, Japan

[8] Research Center for Dynamic Living Systems, Kyoto University, Kyoto 606-8501, Japan

[9] AMED-CREST, AMED, Otemachi 1-7-1, Chiyoda-ku, Tokyo 100-0004, Japan

[*] Correspondence: ryusuke-niwa@tara.tsukuba.ac.jp

Keywords

Drosophila, glucose, gut epithelium, immune system, lifespan, scopoletin

Abstract

Organisms can generally be divided into two groups: generalists that consume various types of food, and specialists that consume specific types of food. However, it remains unclear how specialists adapt to only the limited nutritional conditions present in nature. In this study, we addressed this question by focusing on *Drosophila* fruit flies. The generalist *Drosophila melanogaster* can consume a wide variety of foods that contain high glucose levels. In contrast, the specialist *Drosophila sechellia* consumes only the Indian mulberry, known as noni (*Morinda citrifolia*), which contains relatively little glucose. We showed that the lifespan of *D. sechellia*, was significantly shortened under a high-glucose diet, but this effect was not observed for *D. melanogaster*. In *D. sechellia*, a high-glucose diet induced disorganization of the gut epithelia and visceral muscles, which are associated with abnormal indigestion and constipation. RNA-sequencing analysis revealed that many immune-responsive genes were suppressed in the guts of *D. sechellia* fed a high-glucose diet compared to those fed a control diet. Consistent with this difference in gene expression, the abundance of the gut microbiota was altered in *D. sechellia* under high-glucose diet conditions. Additionally, high glucose-induced phenotypes were restored by the addition of tetracycline or scopoletin, a major nutritional component of noni, each of which suppresses gut bacterial growth. We propose that, in *D. sechellia*, a high-glucose diet impairs gut immune function, which leads to abnormal growth of gut bacteria, the disorganization of the gut epithelial structure, and a shortened lifespan.

INTRODUCTION

In nature, there are two types of species regarding the type of food resources they rely on for survival: generalists, who use many resources, and specialists, who are limited to specific resource (Li et al., 2014; Loxdale et al., 2011). Generalists have been shown to have larger niches and geographic ranges than specialists. As specialist species use specific resources, their habitats are more heterogeneous and patchy than those of generalist species (Slatyer et al., 2013). Furthermore, nutritional ecology studies have shown that, due to their narrow variety of food choices, specialists can regulate nutrient balance only by controlling food intake, not by seeking balanced diets (Behmer, 2009; Poissonnier et al., 2018; Raubenheimer & Simpson, 2003). Therefore, specialists are more likely to be affected by nutritional imbalance than generalists. However, it remains unclear how specialists adapt to only the limited nutritional conditions that are specific for survival.

Fruit flies belonging to the genus *Drosophila* can include both generalist and specialist species; however, both types of *Drosophila* species are thought to have evolved from a common ancestor (Anholt, 2020; Saisawang & Ketterman, 2014). For example, *D. melanogaster* and *D. simulans* are generalists that consume various foods (Markow, 2015; Markow & O'Grady, 2008), while *D. sechellia* is a specialist that is geographically restricted to the Seychelles Islands; however, all three species belong to the same taxonomic clade, the *melanogaster* species subgroup. *D. sechellia* only consumes the Indian mulberry *Morinda citrifolia*, commonly known as noni (Salazar-Jaramillo & Wertheim, 2021), which contains few carbohydrates (Watanabe et al., 2019) (Fig. S1). Such differential food choice between *D. sechellia* and other species of the *melanogaster* subgroup is reflected by the differences in their detoxification ability and chemoattraction characteristics. For example, noni is toxic to *D. melanogaster* and *D.*

simulans (Jones, 2001), whereas *D. sechellia* is resistant to the toxins, partly because of the presence of the detoxifying gut bacteria *Lactiplantibacillus* (Heys et al., 2019). In addition, *D. melanogaster* and *D. simulans* are repelled by the octanoic acid and n-caproic acid present in noni, whereas *D. sechellia* is attracted to these fatty acids (Auer et al., 2021; Higa & Fuyama, 1993; Lanno et al., 2017; López et al., 2017; Matsuo et al., 2007; Prieto-Godino et al., 2017; Salazar-Jaramillo & Wertheim, 2021). However, when *D. melanogaster* ingests gut microbes that are usually harbored in *D. sechellia* guts, *D. melanogaster* is attracted to octanoic acid (Heys et al., 2021). Therefore, it is hypothesized that *D. sechellia* and its gut microbes may be evolutionarily and ecologically specialized to noni, allowing *D. sechellia* to be able to avoid interspecific competition and achieve reproductive success.

Previous studies have investigated how *D. melanogaster* and *D. sechellia* adapt at a molecular level to different nutritional conditions. When two species of *Drosophila* larvae are fed diets with different carbohydrate-to-protein ratios, the diet with a higher carbohydrate-to-protein ratio decrease the survival rate of *D. sechellia* during larval development (Watanabe et al., 2019). Moreover, when adults of the two *Drosophila* species are fed these diets after eclosion, the diet with a higher carbohydrate-to-protein ratio results in reduced egg production and a shortened lifespan in *D. sechellia*, but not in *D. melanogaster* (Watada et al., 2020).

The difference in the effects of the distinct diets can be partly explained by the differences in the carbohydrate-responsive pathways between *D. melanogaster* and *D. sechellia*. *D. melanogaster* has active carbohydrate-responsive pathways, including the TGF-β/activin signaling pathway (Chng et al., 2014, 2017; Ghosh & O'Connor, 2014; Mattila & Hietakangas, 2017; Mattila et al., 2015; Watanabe et al., 2019). In contrast, the noni-consuming *D. sechellia* has lost this type of mechanism during evolution and

has become hypersensitive to a carbohydrate-rich diet (Melvin et al., 2018; Watanabe et al., 2019). However, the physiological mechanism behind high-carbohydrate adaptation has only been validated in larvae and has not been elucidated in adults. Thus, in this study, we aimed to investigate the effect of a high-glucose diet on *D. melanogaster* and *D. sechellia* adults and examine the mechanistic differences in high-glucose adaptation between these two closely related *Drosophila* species.

MATERIALS AND METHODS

Fly husbandry

The wild-type *D. melanogaster* strain Oregon R, which has been maintained in RN's lab for over 14 years, was used in this study. Wild-type *D. sechellia* strain K-S10 was obtained from KYORIN-Fly (Fly Stocks of Kyorin University, Japan). *D. melanogaster* and *D. sechellia* were both reared on a standard diet (see below) at 25 °C with a light cycle of 12 h light and 12 h dark. In this study, we used virgin females for all assays.

Fly Diets

The control diet (CD) stock was a mixture of 100 mL of distilled water, 10 g glucose, 9 g of cornmeal, 4 g dry yeast, 1 g agar, and 300 μL propionic acid, for a glucose concentration of 8% (w/w). The high-glucose diet (HGD) stock was a mixture of 100 mL distilled water, 50 g glucose, 9 g cornmeal, 4 g dry yeast, 1 g agar, and 300 μL propionic acid, leading to 30% (w/w) glucose. To prepare tetracycline-supplemented diet, 200 mg of tetracycline (product no: T3383; Sigma-Aldrich) was added to 100 g of CD or HGD. We also prepared a stock of scopoletin-supplemented diet, which consisted of 100 g of CD or HGD with 11.7 mg scopoletin (product no: S0367; Tokyo Kasei Kogyo). All diets were stored at 4 °C.

131

132 ***Drosophila* lifespan assay**

133 Lifespan was measured in unmated females. A total of 10–20 adults were reared in 21
134 mL mini-vials (product no: 58.487; Sarstedt, Nümbrecht, Germany) containing
135 approximately 3 g of food. The food was refreshed every 3 d.

136

137 **Measurement of triacylglycerol (TAG)**

138 Five unmated females from each group were collected on the fifth day after eclosion.
139 The flies were homogenized in 500 μL of PBS (phosphate-buffered saline) with 0.2%
140 Triton X-100 using BioMasher (Nippi, Yokohama, Japan), and they were incubated in a
141 heat block at 70 °C for 10 min. The samples were centrifuged at 17,800 × *g* for 10 min
142 at 4 °C, and then the supernatant was collected. Ten microliters of the supernatant were
143 used for protein quantification via a Bradford assay with a Coomassie brilliant blue
144 (CBB) protein assay solution (product no: 29449-15; Nacalai Tesque, Kyoto, Japan).
145 The amount of TAG in the whole body was measured in 10 μL of supernatant using a
146 serum triglyceride measurement kit (product no: TR0100; Sigma-Aldrich, St. Louis,
147 MO, USA). The amount of free glycerol was subtracted from the measured value, and
148 the subtracted value was normalized to the amount of protein.

149

150 **Measurement of circulating glucose level**

151 We extracted the body fluids from *Drosophila* adults to measure the concentration of
152 glucose. The thoraxes of 30–40 adult females (5–6 days after eclosion) were punctured
153 with a tungsten needle, placed in 1.5 mL tubes, and centrifuged to collect the body
154 fluids. The samples were centrifuged at 9,000 × *g* for 10 min.

155 The body fluid collected by centrifugation (1 μL) was mixed with 99 μL of

156 trehalase buffer (5 mM Tris-HCl, 137 mM NaCl, 2.7 mM KCl [pH 6.6]). The samples
157 were incubated at 70 °C for 5 min. The glucose level of the body fluids was measured
158 by testing 30 μL of the resulting supernatant with a Glucose Assay Kit (product no:
159 GAGO20-1KT; Sigma-Aldrich).
160
161 **Evaluation of stone formation in the Malpighian tubules**
162 To determine the level of stone formation in the Malpighian tubules, we observed the
163 tubules of unmated females reared on CD or HGD at five days post-eclosion. The
164 Malpighian tubules were dissected in PBS. The level of stone formation in the
165 Malpighian tubules was evaluated on a five-point scale (0–4), as previously described
166 (van Dam et al., 2020). To evaluate the level of stone formation under each dietary
167 treatment, we calculated the average score for each treatment group.
168
169 **Measurement of intestinal alkaline phosphatase activity**
170 To investigate the barrier function of the gut, we examined the activity of intestinal
171 alkaline phosphatase (IAP), an intestinal mucosal defense factor that influences
172 intestinal permeability, as previously described (Pereira et al., 2018). To measure IAP
173 activity, we used para-nitrophenyl phosphate (pNPP; product no: P0757S; New England
174 Biolabs, Ipswich, MA, USA), a general phosphatase chromogenic substrate, as
175 previously described (Pereira et al., 2018). The guts of approximately five unmated
176 females at five days post-eclosion were dissected in PBS and homogenized in 160 μL of
177 reaction solution (25 mM sodium acetate [pH 5.0], 10 mM pNPP, 1 mM DTT, 20%
178 glycerol) with a protease inhibitor cocktail (cOmplete Mini EDTA-free tablets, product
179 no: 11836170001; Roche, Basel, Switzerland). The homogenates were thoroughly
180 mixed and incubated at 30 °C for 50 min. To stop the reaction, 125 μL of 0.32 M NaOH

was added to 75 µL of the reaction solution, and its absorbance was measured at 405 nm (Niwa et al., 2002). To measure the amount of protein in each sample, 125 µL of CBB protein assay solution was added to 75 µL of the reaction solution, and the absorbance was measured at 595 nm. The absorbance at 405 nm was normalized according to the protein content.

Feeding experiment with blue dye

Blue dye (Erioglaucine; product no: 861146; Sigma-Aldrich) was mixed with the diet to a concentration of 0.16%. Flies were allowed to feed on the diet with blue dye for 24 h. Then, the flies were homogenized in 200 µL PBS, and the number of adults used for homogenization was noted. The homogenate was centrifuged at 17,800 × *g* for 10 min. Next, 90 µL of the supernatant was dispensed into each well of a 96-well plate. The absorbance at 625 nm was measured and the obtained value was normalized according to the number of guts used.

Calcofluor White staining

The guts of unmated females at five days post-eclosion were dissected in 50 mM Tris-HCl. The dissected guts were placed on a glass slide, 100 µL of Calcofluor White stain (product no: 18909; Sigma-Aldrich) was placed onto the tissue, and 100 µL of 10% KOH solution was added. The glass slide was lightly shaken to mix the solutions. After mixing, a glass cover was placed on the slide. The samples stained with Calcofluor White were observed under UV light at λ_{ex} = 355 nm.

Counting of feces

Newly eclosed, unmated females were reared under CD or HGD conditions for five

days. Twenty flies were then placed in empty vials without any food for 4 h, and the flies originally reared on CD or HGD were left to feed on the same food stained with blue dye (Erioglaucine; final concentration of 0.16%) for three hours. The flies were then transferred into new empty vials without any food, and the number of feces droplets on the vial walls was counted.

Immunohistochemistry

Unmated females at five days post-eclosion were dissected in PBS. The dissected guts were fixed in 4% paraformaldehyde/PBS for 1 h and the tissue was washed three times with PBT (PBS with 0.1% Triton X-100). After washing, the tissues were rinced with in a graded series of ethanol solutions (10%, 30%, and 70% ethanol), and then further dehydrated with 100% ethanol for 15 min. The dehydrated guts were washed three times with PBT and blocked with blocking solution (2% bovine serum albumin [BSA]/PBT) for 1 h at room temperature. The blocked tissues were treated with the following primary antibodies diluted in blocking solution and incubated at 4 °C overnight: mouse anti-Coracle (Cora) antibody (1:100, DSHB C615.16), mouse anti-Discs large (Dlg) antibody (1:50; Developmental Studies Hybridoma Bank [DSHB] 4F3), anti-Mesh antibody (1:1,000) (Izumi et al., 2016), rabbit anti-Phospho-Ezrin [Thr567]/Radixin [Thr564]/Moesin [Thr558] (pEzrin) antibody 48G2 (1:200; product no: 3726S; Cell Signaling Technology, Danvers, MA, USA), rabbit anti-tachykinin (Tk) antibody (1:50; a gift from Jan Veenstra) (Veenstra et al., 2008), and anti-Tetraspamin-2A (Tsp2A) antibody (1:1,000) (Izumi et al., 2016). After primary antibody treatment, the tissues were washed with PBT. The samples were then incubated with a blocking solution containing goat anti-mouse IgG conjugated with Alexa Fluor 488 (1:200; product no: A32723; Thermo Fisher Scientific, Waltham, MA, USA) or goat anti-rabbit

IgG conjugated with Alexa Fluor 555 (1:200; product no: A32732; Thermo Fisher Scientific) and phalloidin conjugated with Alexa Fluor 546 (1:200; product no: A22283; Thermo Fisher Scientific) under light-shielded conditions for 2 h at room temperature. The tissues were then washed with PBT for 30 min, with nuclear staining with 4',6-diamidino-2-phenylindole (DAPI; 1:1000, diluted in PBT) performed at 15 min. FluorSave reagent (product no: 345789; Merck Millipore, Burlington, MA, USA) was used for mounting the samples on glass slides.

Electron microscopy

Unmated females at five days post-eclosion were dissected in ultrapure water (Milli-Q; Sigma-Aldrich). The dissected guts were fixed in a mixture of 2% paraformaldehyde, 2.5% glutaraldehyde, and 0.1 M cacodylate [pH 7.4] for 1 h at room temperature. After fixation, the guts were washed in 0.1 M cacodylate buffer and post-fixed in 1% osmium tetroxide with 0.1 M cacodylate buffer [pH 7.4] for 1 h at room temperature. The guts were washed with distilled water and stained with 0.5% uranyl acetate for 2 h at room temperature. After three washes with distilled water, the guts were dehydrated in a graded series of ethanol solutions (65%, 75%, 85%, 95%, and 99.5%) and transferred to 100% ethanol. The guts were then soaked in propylene oxide, transferred to a 1:1 mixture of propylene oxide and Quetol 812 resin (Nisshin-EM, Tokyo, Japan), and embedded in Epon 812 resin. Ultrathin sections of approximately 60-nm thickness were collected on copper grids; stained with 0.5% uranyl acetate; and then stained with a lead solution containing 1% lead citrate, 1% lead nitrate, and 2% sodium citrate (Sato, 1968). The sections were washed with distilled water and dried. The sections were observed using a JEM-1010 electron microscope (JEOL, Tokyo, Japan) equipped with a Veleta TEM CCD camera (Olympus, Tokyo, Japan) at an accelerating voltage of 80 kV.

RNA-sequencing (RNA-seq) and gene ontology analysis

RNA-seq was performed on unmated females of the two *Drosophila* species at five days post-eclosion to analyze the genes whose expression was altered. Total RNA was extracted using RNAiso Plus (product no: 9101; TaKaRa Bio; Kusatsu, Shiga, Japan) and an RNeasy Mini kit (product no: 74104; QIAGEN, Hilden, Germany). An average of 20 million reads was sequenced for each biological replicate. For quantification of gene expression, fastq files containing the raw sequence reads were assessed for quality using FASTQC. The sequences were trimmed at 1 nt from the 3′ end and at the adaptor sequences, and reads with a length of <20 nt were trimmed from the raw single-end reads using Trim Galore 0.6.4 (Babraham Bioinformatics, Cambridge, UK). Reads were mapped using HISAT2 (version 2.1.0) (Kim et al., 2019) to the BDGP *D. melanogaster* genome (dm6) downloaded from FlyBase (Larkin et al., 2021) or the *D. sechellia* genome (GCF_004382195.1) from the datasets of the National Center for Biotechnology Information (NCBI), USA. The gtf files (dmel-all-r6.30.gtf) were downloaded from FlyBase for *D. melanogaster* and the National Center for Biotechnology Information (NCBI, USA) database (NCBI release 101) for *D. sechellia*. Samtools (version 1.9) (Li et al., 2009) and Stringtie (version 2.0.6) (Pertea et al., 2016) were used to sort, merge, and count the number of reads mapped to each gene. The number of trimmed mean of M-values (TMM)-normalized fragments per kilobase of combined exon length per one million of total mapped reads (TMM-normalized FPKM value) was calculated using R (version 3.6.1), Ballgown (version 2.18.0) (Pertea et al., 2016), and edgeR (version 3.28.0) (McCarthy et al., 2012; Robinson et al., 2010). Genes with a Benjamini–Hochberg false discovery rate (FDR) lower than 0.01 were identified as differentially expressed genes (DEGs).

D. melanogaster orthologs of each *D. sechellia* gene were downloaded from FlyBase (dmel_orthologs_in_drosophila_species_fb_2021_03.tsv). *D. sechellia* DEGs and *D. melanogaster* orthologs of *D. sechellia* DEGs were uploaded to Metascape (Zhou et al., 2019) and analyzed. If a *D. sechellia* gene was not orthologous to any *D. melanogaster* gene annotated by FlyBase, we manually searched for *D. melanogaster* ortholog(s) using the NCBI database and assigned orthologous relationships if we found any orthologs.

Colony formation assay

A colony formation assay was conducted to determine the amount of gut bacteria present in adult *Drosophila*. Five bacterial culture media were used: brain heart infusion (BHI) broth (18.5 g Bacto BHI [Becton Dickinson 237500], 7.5 g agar, and 500 mL distilled water); lysogeny broth (LB) (10 LB tablets with agar [Lennox; Sigma-Aldrich L7025] and 483 mL distilled water); de Man, Rogosa, and Sharpe (MRS) broth (26 g MRS broth [Oxoid CM0359], 7.5 g agar, and 500 mL distilled water); liver infusion broth (LIB) (Difco LIB [Becton Dickinson 226920], 7.5 g agar, and 500 mL distilled water); and Mannitol (12.5 g D-Mannitol [Sigma-Aldrich M4125], 1.5 g Bacto Peptone [Beckton Dickinson 211677], 2.5 g select yeast extract [Sigma-Aldrich Y1000], 7.5 g agar, and 500 mL distilled water). The guts of 10 HGD-treated unmated females at five days post-eclosion were dissected in 50 mM Tris-HCl. The dissected guts were placed in 250 μL of each liquid medium, and the tissues were mashed using a BioMasher (Nippi). The gut sample solutions were diluted to 1–1/16. After five days of incubation, the number of colonies growing on each plate was counted, and the colony-forming units (CFU) were calculated. The number of replicates used is described in the individual figure legends.

306

307 **Visualization of lipid droplets in the gut**

308 Staining was performed using LipidTOX, as previously described (Bailey et al., 2015).
309 Unmated females at five days post-eclosion were dissected in PBS. The dissected guts
310 were fixed in 4% paraformaldehyde/PBS for 40 min. The fixed tissues were washed
311 three times with PBS and 0.2% TritonX-100. After washing, the guts were stained with
312 LipidTOX and DAPI (diluted 1:1000 in PBS and 0.2% Triton X-100) for 2 h under
313 light-shielded conditions. FluorSave reagent (Merck Millipore) was used to mount the
314 samples on glass slides.

315

316 **RESULTS**

317 ***D. sechellia* lifespan is shortened under high-glucose conditions**

318 First, we examined the effect of a high-glucose diet on the adult lifespans of *D.*
319 *melanogaster* and *D. sechellia*. In all assays, we used virgin females to exclude the
320 possibility of species-specific contributions of egg laying to lifespan (Watada et al.,
321 2020). We grew wild-type strains of these *Drosophila* species from the larval to pupal
322 stage on a control diet (CD) with 8% (w/w) glucose. We then transferred the newly
323 eclosed adult flies into CD or high-glucose diet (HGD) treatment groups, the latter of
324 which was prepared by adding excess glucose to the CD, leading to 30% (w/w) glucose.
325 This methodology was chosen because several previous studies have utilized a 30%
326 glucose diet (May et al., 2019; Musselman & Kühnlein, 2018; Musselman et al., 2011;
327 Na et al., 2013). We found no change in the lifespan of *D. melanogaster* between the
328 CD and HGD groups (Fig. 1A). In contrast, HGD drastically shortened the lifespan of
329 *D. sechellia* compared to CD (Fig. 1B), suggesting that *D. melanogaster* and *D.*
330 *sechellia* are tolerant and sensitive to diets with a high glucose content, respectively.

Food intake, TAG and blood glucose levels, and tubular stone formation are not associated with the shortened lifespan of *D. sechellia* reared on HGD

We next investigated how behavioral and physiological responses to HGD differed between *D. melanogaster* and *D. sechellia*. We found no differences in food intake between these species (Fig. S2A), suggesting that excessive glucose intake does not account for the shortened lifespan induced by HGD in *D. sechellia*.

It is well known that high-sugar diets result in increased TAG levels, blood glucose levels, and stone formation in the Malpighian tubules of *D. melanogaster*, and these factors are all associated with a shortened lifespan (van Dam et al., 2020; Hofbauer et al., 2021; Liao et al., 2021). Therefore, we examined whether these phenotypes could be observed in *D. sechellia* under HGD conditions. We found that TAG levels and blood glucose concentrations were elevated in both *D. melanogaster* and *D. sechellia* under HGD (Fig. S2B, C). In contrast, the level of Malpighian tubule stone formation was not enhanced, but was suppressed in *D. sechellia* compared to *D. melanogaster* under HGD (Fig. S3). These results suggest that TAG levels, blood glucose levels, and tubular stone formation are unlikely to be responsible for the shortened lifespan of *D. sechellia* under HGD conditions.

Disrupted gut epithelial structure in *D. sechellia* reared on HGD

Previous studies have shown that intestinal structure and the gut environment, which includes proper maintenance of the gut epithelium, gut immune system, and gut microbiota, affect the lifespan of *D. melanogaster* (Biagi et al., 2016; Biteau et al., 2010; Boehme et al., 2021; Claesson et al., 2012; Guo et al., 2014; Keebaugh et al., 2018; Li et al., 2016; Loch et al., 2017; Mackowiak, 2013). However, the relationship

between gut function and lifespan in *D. sechellia* has not been examined. Therefore, we examined whether and how the intestinal structure and environment of *D. sechellia* were altered under HGD conditions. First, we visualized the nuclei, actin cytoskeleton, apical surface, and septate junctions of the gut epithelial structure. There were no visible changes in the cell morphology or the sheet structure of the gut epithelia of *D. melanogaster* between CD and HGD conditions, as these insects exhibited uniform monolayer epithelia (Fig. 2A and Fig. S4). In contrast, disorganization of gut epithelia occurred in *D. sechellia* under HGD but not CD conditions (Fig. 2A and Fig. S4). Specifically, the gut epithelia of *D. sechellia* were frequently undulating under HGD conditions (Fig. 2A). Given that the posterior midgut exhibited higher frequencies of disorganization than the anterior midgut, we scored the degree to which the epithelium undulated. We confirmed that the gut epithelium was severely disorganized in *D. sechellia* under HGD conditions (Fig. 2B). Furthermore, electron microscopy revealed that two cells were often aligned along the apicobasal axis of the epithelium (Fig. 2C). These abnormalities were not observed in *D. melanogaster* under either CD or HGD conditions or in *D. sechellia* under CD conditions (Fig. 2A–C).

We also found that the distributions of septate junction proteins (Dlg, Tsp2A, Mesh, and Cora) and an apical marker protein (pEzrin) were altered in *D. sechellia* reared on HGD, probably due to intestinal epithelial undulation (Fig. 2A and Fig. S4). Nevertheless, the apicobasal polarity of the *D. sechellia* gut epithelium under HGD conditions was not severely affected, as Dlg, Dsp2A, Mesh, and Cora were still localized in the basolateral region, and pEzrin was localized at the apical surface (Fig. 2A and Fig. S4). These results suggest that, in *D. sechellia*, HGD affects gut epithelial morphology independently of apicobasal polarity.

We also investigated whether the intestinal muscle fibers surrounding the gut

epithelia were affected by a high-glucose diet. In *D. melanogaster*, there were no changes in the myofiber structure of the two types of visceral muscle (i.e., circular and vertical visceral muscles) between CD and HGD conditions (Fig. 2D). In contrast, in the guts of *D. sechellia* reared on HGD, disorganized myofibers were observed in both types of visceral muscle (Fig. 2D). Based on these results, we speculate that HGD-induced disorganization of the gut epithelia and visceral muscles might be responsible for the shortened lifespan of *D. sechellia*.

As gut barrier dysfunction is frequently associated with a shortened lifespan (Clark et al., 2015; Pereira et al., 2018; Rera et al., 2012), we evaluated whether gut barrier function was impaired in *D. sechellia* reared on HGD. For this purpose, we measured the activity of IAP, an intestinal mucosal defense factor that influences gut permeability (Pereira et al., 2018). However, we found that IAP activity was unchanged under CD and HGD in both species (Fig. S5), suggesting that the gut epithelial disorganization of *D. sechellia* under HGD conditions does not seem to lead to gut barrier dysfunction.

Diet-derived dry yeast cell particles accumulated in the gut lumen of *D. sechellia* reared on HGD

Previous studies have reported that the deformation of muscle fibers surrounding the gut may lead to the disability of gut peristalsis, impairing the digestion and absorption of ingested food (Aghajanian et al., 2016; Schröter et al., 2006). Therefore, we expected that the disrupted epithelial structure of the gut might influence the enteral contents in the gut lumen of *D. sechellia* reared under HGD. This expectation was supported by our staining experiment with Calcofluor White, which binds to cellulose and chitin in bacterial and fungal cell walls (Monheit et al., 1984). We realized that Calcofluor White

406 can also be used to visualize dry yeast cell particles (5–6 μm diameter), which were
407 used to prepare the *Drosophila* diets. (Fig. S6A). In the gut lumens of *D. sechellia* fed
408 with HGD, aberrant enrichment of 5–6 μm-diameter particles stained with Calcofluor
409 White was observed (Fig. 2E). In contrast, 5–6 μm-diameter particles were hardly
410 observed in *D. melanogaster* in either CD or HGD conditions or in *D. sechellia* under
411 CD conditions. However, there were smaller (0.1–4 μm) particles stained with
412 Calcofluor White for these treatments, which likely corresponded to bacteria or
413 remnants of digested dry yeast in the lumen (Fig. 2E). We confirmed that the majority of
414 the large particles were dry yeast cell particles, as there were remarkably fewer 5–6 μm-
415 diameter particles in the gut lumen of *D. sechellia* reared on a diet without dry yeast
416 (Fig. S6B). Moreover, the amount of feces was significantly reduced in both species
417 under HGD conditions, with no feces observed for *D. sechellia* under HGD (Fig. 2F).
418 These results imply that the disorganization of the gut epithelia and visceral muscles of
419 *D. sechellia* under HGD conditions leads to the abnormal accumulation of consumed
420 food in the gut lumen owing to impaired gut digestive function.
421
422 **Expression of genes activating gut immune function is downregulated in *D.***
423 ***sechellia* reared on HGD**
424 Next, we characterized the HGD-induced gut dysfunction in *D. sechellia* using
425 transcriptomic analysis. We conducted an RNA-seq analysis of the guts of *D.*
426 *melanogaster* and *D. sechellia* reared on CD and HGD. We focused on genes whose
427 expression levels were altered more than two-fold in HGD compared to CD and whose
428 FDR values were less than 0.01 (Fig. 3A and Table S1). We then performed a gene
429 ontology (GO) analysis of the DEGs. We found that a certain number of downregulated
430 genes were classified into GO terms related to carbohydrate and lipid metabolism (Fig.

3B). Therefore, the gene expression profile of such nutritional metabolism cannot account for the HGD-induced gut phenotypes of *D. sechellia.*

In contrast, one characteristic difference between the two species was the classification of GO terms related to immune function (Fig. 3B). In *D. melanogaster* reared under HGD, the expression of genes classified as GO:0002814 was decreased (Figure 3B and Table S1). GO:0002814 includes genes related to the "negative regulation of the biosynthetic process of antibacterial peptides active against gram-negative bacteria," such as genes encoding Bomanin and Peptidoglycan recognition proteins, suggesting that gut immune function might be enhanced in *D. melanogaster* under HGD conditions. In contrast, in *D. sechellia*, the expression of genes classified as GO:0009607 and GO:0051607 was significantly decreased under HGD conditions (Fig. 3B and Table S2). GO:0009607 and GO:0051607 include genes related to "response to biotic stimuli" and "defense against viruses," respectively, such as genes encoding antimicrobial peptides (the Turandot family of proteins, Defensin, Drosocin, Metchnikowin, and some Immune-induced peptides) and genes related to the Toll pathway and the immune deficiency (IMD) pathway. These results suggest that, in contrast to *D. melanogaster*, *D. sechellia* gut immune function is impaired when reared on HGD.

A previous study reported that *D. melanogaster* with mutations in the IMD pathway had large lipid droplets in the gut epithelial cells due to an imbalance of the gut bacteria, and that the formation of these droplets was caused by the suppressed production of the peptide hormone tachykinin (Tk) in enteroendocrine cells (Kamareddine et al., 2018). Therefore, we examined whether intestinal lipid droplets were altered in *D. sechellia* under HGD conditions using LipidTOX staining. The lipid droplets were larger in the gut epithelium of *D. sechellia* reared under HGD compared

456 to those in *D. melanogaster* (Fig. 3C). However, the protein level of Tk in
457 enteroendocrine cells did not change in either *D. melanogaster* or *D. sechellia* under CD
458 or HGD conditions (Fig. S7). Therefore, the large lipid droplet formation in *D. sechellia*
459 is quite similar to the lipid droplet formation mediated by the IMD pathway in *D.*
460 *melanogaster*, though it may be generated by a different mechanism than the Tk-
461 dependent mechanism.
462
463 **Increased amount of gut bacteria in *D. sechellia* on HGD**
464 Considering that many positive regulators of immune responses have downregulated
465 expression in the gut of *D. sechellia* reared on HGD, we expected that *D. melanogaster*
466 and *D. sechellia* might differ in the quantity and/or quality of the gut microbiota. To test
467 this hypothesis, we performed colony formation assays using five types of bacterial
468 culture media to examine the amount of gut bacteria in *D. melanogaster* and *D.*
469 *sechellia* reared on HGD. We found that *D. sechellia* guts yielded more colonies than
470 those of *D. melanogaster* on LB, BHI, MRS, and Mannitol media, but not on LIB (Fig.
471 S8, Fig. 4A). These results suggest that at least some gut bacteria overgrow in the gut of
472 *D. sechellia* as compared to *D. melanogaster* under HSD conditions, as expected.
473
474 **Addition of tetracycline to HGD restores the shortened lifespan of *D. sechellia***
475 Based on the above results, we hypothesized that *D. sechellia*-specific gut bacteria
476 might be involved in shortening the lifespan of *D. sechellia* under HGD conditions. To
477 test this hypothesis, we examined whether the shortened lifespan of *D. sechellia* under
478 HGD conditions was suppressed when the flies were fed tetracycline, an antimicrobial
479 agent (Chopra & Roberts, 2001). A colony formation assay confirmed that the
480 tetracycline treatment significantly suppressed bacterial growth in *D. melanogaster* and

D. sechellia guts (Fig. 4A).

Next, we measured the lifespan of both *Drosophila* species after being fed CD and HGD with the addition of tetracycline. The lifespan of *D. melanogaster* was extended by the tetracycline treatment (Fig. 4B), which aligns with the effect observed in a previous study (Obata et al., 2018). Interestingly, tetracycline treatment extended the lifespan of *D. sechellia* to some extent even when under HGD conditions (Fig. 4B). Therefore, it is likely that the gut bacteria are at least in some part responsible for the shortened lifespan of *D. sechellia* under HGD conditions.

We also observed the gut epithelial structures of *Drosophila* given diets with tetracycline. In *D. melanogaster*, there was no obvious change in the gut epithelial structure with the addition of tetracycline (Fig. 4C, D). In contrast, tetracycline suppressed the disruption of the gut epithelial structure in *D. sechellia* under HGD conditions, as the gut epithelia under the tetracycline treatment were seldom undulating (Fig. 4C, D). Additionally, in the guts of *D. sechellia*, the size of the lipid droplets became smaller, and lipid accumulation was suppressed (Fig. 4E). In contrast, there was no dramatic change in the size of the lipid droplets in the guts of *D. melanogaster* fed HGD with tetracycline. Moreover, tetracycline treatment led to a reduction in the number of Calcofluor White-positive 5–6 μm particles that corresponded to dry yeast in the guts of *D. sechellia* under HGD conditions (Fig. 4F, G). These results suggest that gut bacteria are crucial for gut epithelial disorganization and food digestion in *D. sechellia* under HGD conditions.

Addition of scopoletin restores the shortened lifespan and the disrupted gut epithelial structure *D. sechellia* under HGD conditions

D. sechellia is a specialist that only consumes noni (Anholt, 2020; Saisawang &

Ketterman, 2014). Therefore, from a nutritional perspective, we examined whether the dietary addition of a major nutrient present in noni would affect lifespan. Previous studies have reported that scopoletin, a coumarin, is a major nutrient present in noni that contributes to its antioxidative properties (Tasfiyati et al., 2022). We found that the lifespan of *D. melanogaster* did not change when scopoletin was added to CD and it tended to be shorter when scopoletin was added to HGD (Fig. 5A). In contrast, the addition of scopoletin to HGD extended the lifespan of *D. sechellia*, similarly to the effect of tetracycline (Fig. 5A). These results suggest that scopoletin contributes to the extension of *D. sechellia* lifespans, even under HGD conditions.

We further examined whether scopoletin affected gut bacterial growth and gut epithelial structure. When we cultured gut bacteria from both *D. melanogaster* and *D. sechellia* reared on HGD, scopoletin suppressed the growth of *D. melanogaster* gut bacteria cultured on BHI, LB, and MRS, and it suppressed the growth of *D. sechellia* gut bacteria cultured on all studied bacterial culture media (Fig. 5B). In *D. sechellia,* the addition of scopoletin to HGD restored the disrupted gut epithelial structure, but this did not occur for *D. melanogaster* (Fig. 5C, D). These results indicate that scopoletin, an important component of noni, has a protective effect on survival when *D. sechellia* is fed a high-glucose diet.

DISCUSSION

The results of multiple experiments in this study strongly suggest that abnormal growth of gut bacteria in *D. sechellia* causes a shortened lifespan under HGD conditions. Under HGD conditions, the expression of genes that suppress immune function may be decreased in *D. melanogaster*, leading to maintained or enhanced immune function. As a result, the gut bacteria can be balanced and a healthy gut environment can be

maintained. In *D. sechellia* reared on HGD, the expression of genes that activate immune functions, such as the Turandot genes *defensin*, *drosocin*, *metchnikowin*, and some *immune-induced peptide* genes, is likely suppressed, causing failed activation or maintenance of gut immune function. This situation would result in abnormal gut microbiota, leading to the disorganization of gut epithelial structures and the abnormal accumulation of lipid droplets in epithelial cells (Fig. 6).

Previous studies have uncovered robust carbohydrate-responsive regulatory systems, including TGF-β/activin signaling pathways, that allow *D. melanogaster* larvae to adapt to carbohydrate-rich diets (Chng et al., 2014; Ghosh & O'Connor, 2014; Mattila et al., 2015; Watanabe et al., 2019). In contrast, *D. sechellia* larvae are deficient in these systems and cannot maintain metabolic homeostasis, resulting in reduced adaptation to carbohydrate-rich diets. Therefore, it is plausible that carbohydrate-responsive regulatory systems, such as TGF-β/activin signaling, are dysfunctional in *D. sechellia* adults. However, we found no noticeable differences in the expression of genes related to carbohydrate-responsive systems in the guts of *D. melanogaster* and *D. sechellia.* Further studies are needed to clarify the mechanistic differences in the carbohydrate-responsive systems in adults of *D. melanogaster* and *D. sechellia*, which will be crucial information for understanding the physiological differences between the adults of these two species.

We propose that high glucose levels affect gut immune function in *D. sechellia* but not *D. melanogaster*. However, the mechanistic differences between these two species is currently unclear at the molecular and cellular levels. Future studies should clarify how abnormal gut microbiota leads to the disorganization of the gut epithelium and the shortened lifespan in *D. sechellia* under HGD conditions. The gut microbiota can be altered by unbalanced nutrient intake; such effects have been observed in

mammals under high-carbohydrate conditions (Leeming et al., 2019; Seo et al., 2020). Therefore, it would be intriguing to examine whether an evolutionarily conserved mechanism regulates high-glucose/carbohydrate-induced immune dysfunction. As the abnormal accumulation of large lipid droplets in the gut lumens of *D. sechellia* under HGD conditions is similar to what occurs during loss of IMD function in *D. melanogaster*, we initially expected that this observation in *D. sechellia* might be due to the same cause. However, unlike *D. melanogaster*, there was no change in enteroendocrine Tk protein levels in *D. sechellia* reared on HGD. Unfortunately, it is technologically difficult to conduct a functional analysis of *D. sechellia* using genetic technology to examine whether and how innate immunity pathways are involved in the high glucose-induced gut phenotypes of *D. sechellia*. However, a recent study identified some effective chemical compounds that inhibit the IMD pathway in cultured *D. melanogaster* cells (Tsukada et al., 2020). In future studies, pharmacological approaches using such chemical compounds may be more effective and could be used in functional analyses.

Interestingly, the shortened lifespan and disruption of the gut epithelial structure in flies fed HGD were restored by the addition of scopoletin, a major nutritional component of noni, to the diet. Therefore, nutrients have the potential to help *D. sechellia* survive under unbalanced nutritional conditions. This result implies that specialists can survive in unbalanced environments if their main diet or components of their main diet are present. Previous studies have largely focused on noni toxins when considering the ecological niche of *D. sechellia* and other closely related species (Jones, 2001). In contrast, our study suggests that considering the beneficial aspects of noni may also be important when considering the differences between the specialist *D. sechellia* and generalist *Drosophila* species. In future studies, it will be necessary to

elucidate how scopoletin and other constituents of noni affect gut epithelial structure and gut immune function.

Acknowledgements

We thank Teigo Asai, Koki Kawane, Masanori Toyofuku, Kyoichi Sawamura, Jan Veenstra, KYORIN-Fly (Fly Stocks of Kyorin University), and the Developmental Studies Hybridoma Bank for providing stocks and reagents; Kyoko Furuse and Mikio Furuse for technical assistance in performing electron microscopic observations; Takefumi Kondo and Yukari Sando for their technical support with next-generation sequencing; and Takayuki Kuraishi, Hina Kosakamoto, and Fumiaki Obata for critical advice on phenotypic analyses. T.K. received a fellowship from the Japan Society for the Promotion of Science. We would like to thank Editage (www.editage.com) for their English language editing service.

Footnotes

Author contributions

Conceptualization: M.A., R.N.; Methodology: M.A., Y.D., K.W., Y.H., T.U.; Validation: M.A., T.K., R.N.; Formal analysis: M.A., T.K., Y.I., Q.Q., Y.Y., Y.D., R.N.; Investigation: M.A., T.K., Y.I. Q.Q., Y.Y., Y.D.; Resources: Y.I., Y.D., K.W., Y.H., T.U., R.N.; Data curation: M.A., T.K., Y.I., R.N.; Writing – original draft: M.A., R.N.; Writing – review & editing: All authors; Visualization: M.A, T.K., Y.I., Q.Q., R.N.; Supervision: Y.D., Y.H., T.U., R.N.; Funding acquisition: M.A., Y.I., Y.Y., Y.D., T.U., R.N.

Funding

This work was supported by grants from AMED-CREST, AMED (22gm1110001s0006

606 and 22gm1110001s0306) to T.U. and R.N., JSPS KAKENHI (JP19H03281) to Y.D., and
607 ST SPRING (JPMJSP2124) to Y.Y. This work was also supported by the Advancing
608 Researcher Experience Program of the University of Tsukuba to M.A., and the
609 Cooperative Study Program (21-149) of the National Institute for Physiological
610 Sciences to Y.I. and R.N.
611

612 **Data availability**

613 The raw RNA-seq data generated in this study have been deposited in the DNA Data
614 Bank of Japan Sequence Read Archive database under accession codes DRA013864
615 (data for *D. melanogaster*) and DRA013865 (data for *D. sechellia*).
616

617 **Competing interests**

618 The authors declare no competing or financial interests.
619

620 **References**

621 Aghajanian, P., Takashima, S., Paul, M., Younossi-Hartenstein, A., & Hartenstein, V.
622 (2016). Metamorphosis of the Drosophila visceral musculature and its role in intestinal
623 morphogenesis and stem cell formation. *Dev. Biol.* **420**, 43–59.
624 Anholt, R.R.H. (2020). Chemosensation and Evolution of Drosophila Host Plant
625 Selection. *iScience* **23**, 100799.
626 Auer, T.O., Shahandeh, M.P., & Benton, R. (2021). Drosophila sechellia A Genetic
627 Model for Behavioral Evolution and Neuroecology. *Annu. Rev. Genet.* **55**, 527–554.
628 Bailey, A.P., Koster, G., Guillermier, C., Hirst, E.M.A., MacRae, J.I., Lechene, C.P.,
629 Postle, A.D., & Gould, A.P. (2015). Antioxidant Role for Lipid Droplets in a Stem
630 Cell Niche of Drosophila. *Cell* **163**, 340–353.

631 Behmer, S.T. (2009). Insect herbivore nutrient regulation. *Annu. Rev. Entomol.* **54**, 165–
632 187.
633 Biagi, E., Franceschi, C., Rampelli, S., Severgnini, M., Ostan, R., Turroni, S.,
634 Consolandi, C., Quercia, S., Scurti, M., Monti, D., Capri, M., Brigidi, P., & Candela,
635 M. (2016). Gut Microbiota and Extreme Longevity. *Curr. Biol.* **26**, 1480–1485.
636 Biteau, B., Karpac, J., Supoyo, S., DeGennaro, M., Lehmann, R., & Jasper, H. (2010).
637 Lifespan extension by preserving proliferative homeostasis in Drosophila. *PLOS*
638 *Genet.* **6**, e1001159.
639 Boehme, M., Guzzetta, K.E., Bastiaanssen, T.F.S., et al. (2021). Microbiota from young
640 mice counteracts selective age-associated behavioral deficits. *Nat. Aging* **1**, 666–676.
641 Chng, W. bin A., Sleiman, M.S.B., Schüpfer, F., & Lemaitre, B. (2014). Transforming
642 growth factor β/activin signaling functions as a sugar-sensing feedback loop to
643 regulate digestive enzyme expression. *Cell Rep.* **9**, 336–348.
644 Chng, W. bin A., Hietakangas, V., & Lemaitre, B. (2017). Physiological Adaptations to
645 Sugar Intake: New Paradigms from Drosophila melanogaster. *Trends Endocrinol.*
646 *Metab.* **28**, 131–142.
647 Chopra, I., & Roberts, M. (2001). Tetracycline Antibiotics: Mode of Action,
648 Applications, Molecular Biology, and Epidemiology of Bacterial Resistance.
649 *Microbiol. Mol. Biol. Rev.* **65**, 232–260.
650 Claesson, M.J., Jeffery, I.B., Conde, S., et al. (2012). Gut microbiota composition
651 correlates with diet and health in the elderly. *Nature* **488**, 178–184.
652 Clark, R.I., Salazar, A., Yamada, R., Fitz-Gibbon, S., Morselli, M., Alcaraz, J., Rana,
653 A., Rera, M., Pellegrini, M., Ja, W.W., & Walker, D.W. (2015). Distinct Shifts in
654 Microbiota Composition during Drosophila Aging Impair Intestinal Function and
655 Drive Mortality. *Cell Rep.* **12**, 1656–1667.

van Dam, E., van Leeuwen, L.A.G., dos Santos, E., et al. (2020). Sugar-Induced Obesity and Insulin Resistance Are Uncoupled from Shortened Survival in Drosophila. *Cell Metab.* **31**, 710-725.e7.

Ghosh, A.C., & O'Connor, M.B. (2014). Systemic Activin signaling independently regulates sugar homeostasis, cellular metabolism, and pH balance in Drosophila melanogaster. *Proc. Natl. Acad. Sci. U. S. A.* **111**, 5729–5734.

Guo, L., Karpac, J., Tran, S.L., & Jasper, H. (2014). PGRP-SC2 promotes gut immune homeostasis to limit commensal dysbiosis and extend lifespan. *Cell* **156**, 109–122.

Heys, C., Fisher, A.M., Dewhurst, A.D., Lewis, Z., & Lize, A. (2019). A potential role for the gut microbiota in the specialisation of Drosophila sechellia to its toxic host noni (Morinda citrifolia). *BioRxiv* , doi: 10.1101/526517.

Heys, C., Fisher, A.M., Dewhurst, A.D., Lewis, Z., & Lizé, A. (2021). Exposure to foreign gut microbiota can facilitate rapid dietary shifts. *Sci. Reports 2021 111* **11**, 16791.

Higa, I., & Fuyama, Y. (1993). Genetics of food preference in Drosophila sechellia - I. Responses to food attractants. *Genetica* **88**, 129–136.

Hofbauer, H.F., Heier, C., Saji, A.K. Sen, & Kühnlein, R.P. (2021). Lipidome remodeling in aging normal and genetically obese Drosophila males. *Insect Biochem. Mol. Biol.* **133**, 103498.

Izumi, Y., Motoishi, M., Furuse, K., & Furuse, M. (2016). A tetraspanin regulates septate junction formation in Drosophila midgut. *J. Cell Sci.* **129**, 1155–1164.

Jones, C.D. (2001). The genetic basis of larval resistance to a host plant toxin in Drosophila sechellia. *Genet. Res.* **78**, 225–233.

Kamareddine, L., Robins, W.P., Berkey, C.D., Mekalanos, J.J., & Watnick Correspondence, P.I. (2018). The Drosophila Immune Deficiency Pathway Modulates

Enteroendocrine Function and Host Metabolism. *Cell Metab.* **28**, 449-462.e5.

Keebaugh, E.S., Yamada, R., Obadia, B., Ludington, W.B., & Ja, W.W. (2018). Microbial Quantity Impacts Drosophila Nutrition, Development, and Lifespan. *IScience* **4**, 247–259.

Kim, D., Paggi, J.M., Park, C., Bennett, C., & Salzberg, S.L. (2019). Graph-based genome alignment and genotyping with HISAT2 and HISAT-genotype. *Nat. Biotechnol. 2019 378* **37**, 907–915.

Lanno, S.M., Gregory, S.M., Shimshak, S.J., et al. (2017). Transcriptomic Analysis of Octanoic Acid Response in Drosophila sechellia Using RNA-Sequencing. *G3* **7**, 3867–3873.

Larkin, A., Marygold, S.J., Antonazzo, G., et al. (2021). FlyBase: updates to the Drosophila melanogaster knowledge base. *Nucleic Acids Res.* **49**, D899–D907.

Leeming, E.R., Johnson, A.J., Spector, T.D., & Roy, C.I.L. (2019). Effect of diet on the gut microbiota: Rethinking intervention duration. *Nutrients* **11**, 2862.

Li, H., Handsaker, B., Wysoker, A., Fennell, T., Ruan, J., Homer, N., Marth, G., Abecasis, G., & Durbin, R. (2009). The Sequence Alignment/Map format and SAMtools. *Bioinformatics* **25**, 2078–2079.

Li, H., Qi, Y., & Jasper, H. (2016). Preventing Age-Related Decline of Gut Compartmentalization Limits Microbiota Dysbiosis and Extends Lifespan. *Cell Host Microbe* **19**, 240–253.

Li, S., Jovelin, R., Yoshiga, T., Tanaka, R., & Cutter, A.D. (2014). Specialist versus generalist life histories and nucleotide diversity in Caenorhabditis nematodes. *Proc. R. Soc. B Biol. Sci.* **281**, 20132858.

Liao, S., Amcoff, M., & Nässel, D.R. (2021). Impact of high-fat diet on lifespan, metabolism, fecundity and behavioral senescence in Drosophila. *Insect Biochem. Mol.*

706 *Biol.* **133**, 103495.
707 Loch, G., Zinke, I., Mori, T., Carrera, P., Schroer, J., Takeyama, H., & Hoch, M.
708 (2017). Antimicrobial peptides extend lifespan in Drosophila. *PLoS One* **12**,
709 e0176689.
710 López, J.M.A., Lanno, S.M., Auerbach, J.M., Moskowitz, E.C., Sligar, L.A., Wittkopp,
711 P.J., & Coolon, J.D. (2017). Genetic basis of octanoic acid resistance in Drosophila
712 sechellia: functional analysis of a fine-mapped region. *Mol. Ecol.* **26**, 1148–1160.
713 Loxdale, H.D., Lushai, G., & Harvey, J.A. (2011). The evolutionary improbability of
714 "generalism" in nature, with special reference to insects. *Biol. J. Linn. Soc.* **103**, 1–18.
715 Mackowiak, P.A. (2013). Recycling Metchnikoff: Probiotics, the intestinal microbiome
716 and the quest for long life. *Front. Public Heal.* **1**, 52.
717 Markow, T.A. (2015). The Natural History of Model Organisms: The secret lives of
718 Drosophila flies. *Elife* **4**, e06793.
719 Markow, T.A., & O'Grady, P. (2008). Reproductive ecology of Drosophila. *Funct.*
720 *Ecol.* **22**, 747–759.
721 Matsuo, T., Sugaya, S., Yasukawa, J., Aigaki, T., & Fuyama, Y. (2007). Odorant-
722 Binding Proteins OBP57d and OBP57e Affect Taste Perception and Host-Plant
723 Preference in Drosophila sechellia. *PLOS Biol.* **5**, e118.
724 Mattila, J., & Hietakangas, V. (2017). Regulation of Carbohydrate Energy Metabolism
725 in Drosophila melanogaster. *Genetics* **207**, 1231–1253.
726 Mattila, J., Havula, E., Ripatti, S., Sandmann, T., Hietakangas, V., Suominen, E.,
727 Teesalu, M., Surakka, I., Hynynen, R., Kilpinen, H., Vä, J., Nä Nen, ¨, Hovatta, I., &
728 Kä Kelä, R. (2015). Mondo-Mlx Mediates Organismal Sugar Sensing through the Gli-
729 Similar Transcription Factor Sugarbabe Accession Numbers GSE70980 Mattila et al
730 Article Mondo-Mlx Mediates Organismal Sugar Sensing through the Gli-Similar

Transcription Factor Sugarbabe. *Cell Rep.* **13**, 350–364.

May, C.E., Vaziri, A., Lin, Y.Q., Grushko, O., Khabiri, M., Wang, Q.P., Holme, K.J., Pletcher, S.D., Freddolino, P.L., Neely, G.G., & Dus, M. (2019). High Dietary Sugar Reshapes Sweet Taste to Promote Feeding Behavior in Drosophila melanogaster. *Cell Rep.* **27**, 1675-1685.e7.

McCarthy, D.J., Chen, Y., & Smyth, G.K. (2012). Differential expression analysis of multifactor RNA-Seq experiments with respect to biological variation. *Nucleic Acids Res.* **40**, 4288–4297.

Melvin, R.G., Lamichane, N., Havula, E., Kokki, K., Soeder, C., Jones, C.D., & Hietakangas, V. (2018). Natural variation in sugar tolerance associates with changes in signaling and mitochondrial ribosome biogenesis. *Elife* **7**, e40841.

Monheit, J.E., Cowan, D.F., & Moore, D.G. (1984). Rapid detection of fungi in tissues using calcofluor white and fluorescence microscopy. *Arch Pathol Lab Med* **108**, 616–618.

Musselman, L.P., & Kühnlein, R.P. (2018). Drosophila as a model to study obesity and metabolic disease. *J. Exp. Biol.* **221**, jeb163881.

Musselman, L.P., Fink, J.L., Narzinski, K., Ramachandran, P.V., Hathiramani, S.S., Cagan, R.L., & Baranski, T.J. (2011). A high-sugar diet produces obesity and insulin resistance in wild-type Drosophila. *Dis. Model. Mech.* **4**, 842–849.

Na, J., Musselman, L.P., Pendse, J., Baranski, T.J., Bodmer, R., Ocorr, K., & Cagan, R. (2013). A Drosophila model of high sugar diet-induced cardiomyopathy. *PLOS Genet.* **9**, e1003175.

Niwa, R., Nagata-Ohashi, K., Takeichi, M., Mizuno, K., & Uemura, T. (2002). Control of actin reorganization by Slingshot, a family of phosphatases that dephosphorylate ADF/cofilin. *Cell* **108**, 233–246.

Obata, F., Fons, C.O., & Gould, A.P. (2018). Early-life exposure to low-dose oxidants can increase longevity via microbiome remodelling in Drosophila. *Nat. Commun.* **9**, 975.

Pais, I.S., Valente, R.S., Sporniak, M., & Teixeira, L. (2018). Drosophila melanogaster establishes a species-specific mutualistic interaction with stable gut-colonizing bacteria. *PLOS Biol.* **16**, e2005710.

Pereira, M.T., Malik, M., Nostro, J.A., Mahler, G.J., & Musselman, L.P. (2018). Effect of dietary additives on intestinal permeability in both Drosophila and a human cell co-culture. *Dis. Model. Mech.* **11**, dmm034520.

Pertea, M., Kim, D., Pertea, G.M., Leek, J.T., & Salzberg, S.L. (2016). Transcript-level expression analysis of RNA-seq experiments with HISAT, StringTie and Ballgown. *Nat. Protoc. 2016 119* **11**, 1650–1667.

Poissonnier, L.A., Arganda, S., Simpson, S.J., Dussutour, A., & Buhl, J. (2018). Nutrition in extreme food specialists: An illustration using termites. *Funct. Ecol.* **32**, 2531–2541.

Prieto-Godino, L.L., Rytz, R., Cruchet, S., Bargeton, B., Abuin, L., Silbering, A.F., Ruta, V., Dal Peraro, M., & Benton, R. (2017). Evolution of Acid-Sensing Olfactory Circuits in Drosophilids. *Neuron* **93**, 661-676.e6.

Raubenheimer, D., & Simpson, S.J. (2003). Nutrient balancing in grasshoppers: Behavioural and physiological correlates of dietary breadth. *J. Exp. Biol.* **206**, 1669–1681.

Rera, M., Clark, R.I., & Walker, D.W. (2012). Intestinal barrier dysfunction links metabolic and inflammatory markers of aging to death in Drosophila. *Proc. Natl. Acad. Sci. U. S. A.* **109**, 21528–21533.

Robinson, M.D., McCarthy, D.J., & Smyth, G.K. (2010). edgeR: a Bioconductor

781 package for differential expression analysis of digital gene expression data.
782 *Bioinformatics* **26**, 139–140.
783 Saisawang, C., & Ketterman, A.J. (2014). Micro-plasticity of genomes as illustrated by
784 the evolution of glutathione transferases in 12 Drosophila species. *PLoS One* **9**,
785 e109518.
786 Salazar-Jaramillo, L., & Wertheim, B. (2021). Does Drosophila sechellia escape
787 parasitoid attack by feeding on a toxic resource? *PeerJ* **9**, e10528.
788 Sato, T. (1968). A modified method for lead staining of thin sections. *J. Electron*
789 *Microsc.* **17**, 158–159.
790 Schröter, R.H., Buttgereit, D., Beck, L., Holz, A., & Renkawitz-Pohl, R. (2006). Blown
791 fuse regulates stretching and outgrowth but not myoblast fusion of the circular visceral
792 muscles in Drosophila. *Differentiation* **74**, 608–621.
793 Seo, Y.S., Lee, H. Bin, Kim, Y., & Park, H.Y. (2020). Dietary carbohydrate constituents
794 related to gut dysbiosis and health. *Microorganisms* **8**, 427.
795 Slatyer, R.A., Hirst, M., & Sexton, J.P. (2013). Niche breadth predicts geographical
796 range size: A general ecological pattern. *Ecol. Lett.* **16**, 1104–1114.
797 Tasfiyati, A.N., Antika, L.D., Dewi, R.T., Septama, A.W., Sabarudin, A., & Ernawati,
798 T. (2022). An experimental design approach for the optimization of scopoletin
799 extraction from Morinda citrifolia L. using accelerated solvent extraction. *Talanta*
800 **238**, 123010.
801 Tsukada, K., Shinki, S., Kaneko, A., et al. (2020). Synthetic biology based construction
802 of biological activity-related library of fungal decalin-containing diterpenoid pyrones.
803 *Nat. Commun. 2020 111* **11**, 1830.
804 Veenstra, J.A., Agricola, H.J., & Sellami, A. (2008). Regulatory peptides in fruit fly
805 midgut. *Cell Tissue Res.* **334**, 499–516.

Watada, M., Hayashi, Y., Watanabe, K., Mizutani, S., Mure, A., Hattori, Y., & Uemura, T. (2020). Divergence of Drosophila species: Longevity and reproduction under different nutrient balances. *Genes to Cells* **25**, 626–636.

Watanabe, K., Kanaoka, Y., Mizutani, S., Uchiyama, H., Yajima, S., Watada, M., Uemura, T., & Hattori, Y. (2019). Interspecies Comparative Analyses Reveal Distinct Carbohydrate-Responsive Systems among Drosophila Species. *Cell Rep.* **28**, 2594-2607.e7.

Zhou, Y., Zhou, B., Pache, L., Chang, M., Khodabakhshi, A.H., Tanaseichuk, O., Benner, C., & Chanda, S.K. (2019). Metascape provides a biologist-oriented resource for the analysis of systems-level datasets. *Nat. Commun.* **10**, 1523.

Figure legends

Fig. 1. A high-glucose diet induces a shortened lifespan in *D. sechellia*

Lifespans of (A) *D. melanogaster* and (B) *D. sechellia* reared on a control diet (CD) and high-glucose diet (HGD). The x- and y-axes represent the number of days after eclosion and the survival rate, respectively. The numbers of flies used in the assays are shown in the figure. ***$p < 0.0001$ (Log-rank test). n.s.: not significant.

Fig. 2. A high-glucose diet induces gut epithelial disorganization in *D. sechellia*

(A) Immunohistochemical observation of the gut epithelial structures of *D. melanogaster* and *D. sechellia* reared on a control diet (CD) and high-glucose diet (HGD). The gut epithelia were stained with fluorescent phalloidin (magenta), anti-Discs large (Dlg; green), and DAPI (blue), which were used to visualize actin filaments, septate junctions, and nuclei, respectively. We focused on the R2 region for our observations. The upper and lower parts of each photo correspond to the apical and basal sides of the gut epithelium, respectively. Scale bar: 10 μm.

(B) Frequency of different midgut morphological phenotypes in *D. melanogaster* and *D. sechellia* reared on CD and HGD. We categorized the gut phenotypes into four categories. A normal midgut is defined as zero, and abnormal undulation of the epithelia over the entire midgut region is defined as 3. The abnormal undulation phenotype was most frequently observed in the posterior midgut, though the reason for this was unknown.

(C) Electron microscopy of the gut epithelial structures of *D. melanogaster* and *D. sechellia* reared on CD and HGD. The upper and lower parts of each photo correspond to the apical and basal sides of the gut epithelium, respectively. Scale bar: 10 μm.

(D) Intestinal muscle fibers surrounding the gut epithelia visualized by fluorescent

phalloidin. Scale bar: 100 μm.

(E) Calcofluor White staining for visualization of bacteria, fungi, and dietary dry yeast cell particles. Long and short scale bars: 100 μm and 5 μm, respectively.

(F) Numbers of feces deposits in 1 h from 20 adult female flies of *D. melanogaster* and *D. sechellia* reared on CD and HGD. Notably, no feces were observed from *D. sechellia* reared on HGD in five independent experiments. **p<0.001 (Student's *t*-test with Bonferroni's correction).

Fig. 3. Differences of the transcriptome and lipid droplet formation between control diet (CD) and high-glucose diet (HGD) conditions in *D. melanogaster* and *D. sechellia*

(A) Volcano plots representing the changes in gene expression between CD and HGD conditions in *D. melanogaster* and *D. sechellia*. The annotated gene sets of *D. melanogaster* and *D. sechellia* used in this study were defined based on the FlyBase and NCBI datasets (also see Tables S1 and S2). The x-axis represents binary logarithmic values ($\log_2$) of the fold changes of gene expression (i.e., expression level of each gene under HGD conditions subdivided by that under CD conditions). The y-axis represents logarithmic values ($\log_{10}$) of the false discovery rates (FDR). Blue dots represent differentially expressed genes with $\log_2$FC<-1 and FDR＜0.01. Red dots represent differentially expressed genes with $\log_2$FC>1 and FDR＜0.01.

(B) Significantly enriched Gene Ontology (GO) terms of the differentially expressed genes (shown in blue in [A]). GO terms for each *D. sechellia* gene were assigned based on the information of a *D. melanogaster* ortholog (See Table S2). The GO terms with corrected P-values less than 0.01 were considered significantly enriched by differentially expressed genes. The intensity of the gray bars varies depending on

whether the range of values of $-\log_{10}(P)$ is 2–4, 4–6, 6–8, or 8–10. Asterisks represent GO classifications that include immune-responsive genes.

(C) Lipid droplets visualized by LipidTOX in the gut epithelia of *D. melanogaster* and *D. sechellia* reared on CD and HGD. Red: LipidTOX; blue, DAPI. Scale bar: 100 μm.

Fig. 4. High-glucose diet (HGD)-induced phenotypes are recovered by tetracycline treatment

(A) Colony formation assay using gut lysates derived from *D. melanogaster* and *D. sechellia* reared on HGD with or without tetracycline. The x-axis represents five types of bacteria culture medium: brain heart infusion (BHI), lysogeny broth (LB), liver infusion broth (LIB), Mannitol, and de Man, Rogosa, and Sharpe broth (MRS). The y-axis represents colony formation units (CFU) from 10 plates of each bacterial culture media (mean ± SEM). * $p<0.05$, ** $p<0.01$, and *** $p < 0.001$ (Tukey–Kramer test). n.s.: not significant.

(B) Lifespan of *D. melanogaster* and *D. sechellia* reared on CD and HGD with or without tetracycline. The x- and y-axes represent the number of days after eclosion and the survival rate, respectively. The numbers of flies used in the assays are represented in the figure. ** $p<0.001$ and *** $p < 0.0001$ (Log-rank test). n.s.: not significant.

(C) Immunohistochemical observation of the gut epithelial structures of *D. melanogaster* and *D. sechellia* reared on CD and HGD with or without tetracycline. The gut epithelia were stained with fluorescent phalloidin (magenta), anti-Discs large (Dlg; green), and DAPI (blue) to visualize the actin filaments, septate junctions, and nuclei, respectively. We focused on the R2 region for our observations. The upper and lower parts of each photo correspond to the apical and basal sides of the gut epithelium, respectively. Scale bar: 10 μm.

(D) Frequency of midgut morphological phenotypes in *D. melanogaster* and *D. sechellia* reared on CD and HGD. The four-point (from 0 to 3) scale used to evaluate abnormal epithelial undulation is the same as that shown in Fig. 2B.

(E) LipidTOX visualization of lipid droplets in the gut epithelium of *D. melanogaster* and *D. sechellia* reared on HGD with or without tetracycline. Red: LipidTOX; blue, DAPI. Scale bar: 100 μm.

(F) Calcofluor White staining used to visualize bacteria, fungi, and dietary dry yeast cell particles in HGD conditions with or without tetracycline. Long and short scale bars: 100 μm and 5 μm, respectively.

(G) Distribution of differently sized particles in the guts of *D. melanogaster* and *D. sechellia* reared on CD and HGD. Note that the large particles (diameter of more than 4–5 μm), which mainly corresponded to dietary dry yeast, were reduced by tetracycline treatment in the gut of *D. sechellia*.

Fig. 5. High-glucose diet (HGD)-induced abnormalities of *D. sechellia* are suppressed by scopoletin, a major nutrient in noni

A) Lifespans of *D. melanogaster* and *D. sechellia* reared on CD and HGD, with and without scopoletin. The x- and y-axes represent the number of days after eclosion and the survival rate, respectively. The number of flies used in the assays is shown in the figure. **$p<0.001$ and ***$p<0.0001$ (Log-rank test). n.s.: not significant.

(B) Colony formation assay using gut lysates derived from *D. melanogaster* and *D. sechellia* reared on HGD with or without scopoletin. The x-axis shows the five types of bacterial culture media: brain heart infusion (BHI), lysogeny broth (LB), liver infusion broth (LIB), Mannitol, and de Man, Rogosa, and Sharpe broth (MRS). The y-axis represents the colony formation units (CFU) from six plates of each bacterial culture

medium (mean ± SEM). * $p<0.05$, ** $p<0.01$, and *** $p < 0.001$ Tukey–Kramer test. n.s.: not significant.

(C) Immunohistochemical observation of the gut epithelial structures of *D. melanogaster* and *D. sechellia* reared on CD and HGD, with or without scopoletin. Gut epithelia were stained with fluorescent phalloidin (magenta), anti-Discs large (Dlg; green), and DAPI (blue) to visualize actin filaments, septate junctions, and nuclei, respectively. We focused on the R2 region for our observations. The upper and lower parts of each photograph correspond to the apical and basal sides of the gut epithelium, respectively. Scale bar: 10 μm.

(D) Frequency of the midgut morphological phenotypes of *D. melanogaster* and *D. sechellia* reared on HGD with or without scopoletin. The four-point (from 0 to 3) scale used to evaluate abnormal epithelial undulation is the same as that shown in Fig. 2B. The gut epithelia in *D. sechellia* reared on HGD with scopoletin treatment seldom undulated.

Fig. 6. Hypothesis of the mechanistic differences of high-glucose diet (HGD)-responsive lifespans of *D. melanogaster* and *D. sechellia*

Under HGD conditions, the expression of genes that suppress immune function is decreased in *D. melanogaster*, suggesting that immune function is enhanced or maintained. Consequently, a healthy gut environment can be maintained. In contrast, in *D. sechellia*, the expression of genes that activate immune function under HGD conditions is suppressed, resulting in an unbalanced quantity and diversity of the gut bacteria. This causes an unhealthy gut environment, leading to a shortened lifespan, disorganization of the gut epithelial structure, abnormal formation of lipid droplets (white circles) in epithelial cells, and the aberrant enrichment of dietary dry yeast cell

943 particles. To a certain extent, such HGD-induced abnormalities can be suppressed by
944 scopoletin. EB, enterblast; EC, enterocyte; EE, enteroendocrine cell; and ISC, intestinal
945 stem cell.
946
947

Supplementary Figures

Fig. S1. Glucose concentrations present in the main diets of *D. melanogaster* and *D. sechellia*

We confirmed that the amount of glucose in noni powder (Miracle Noni Powder 120, Nakazen Inc.) was below the detection limit of our experimental conditions. In contrast, *D. melanogaster* diets, including grapefruit, orange, tomato, and kiwifruit, contained glucose concentrations ranging from 20 to 50 mg/mL. These data are consistent with a previous report describing that noni exhibits a higher protein-to-carbohydrate ratio than the diets of *D. melanogaster* (Watanabe et al., 2019).

Fig. S2. Food intake, triacylglycerol (TAG) levels, and circulating glucose levels do not differ between *D. melanogaster* and *D. sechellia*

(A) Food intake of *D. melanogaster* and *D. sechellia* under control diet (CD) and high-glucose diet (HGD) conditions. Flies were fed diets with blue dye for 24 h. Each dot corresponds to a gut lysate sample prepared by squeezing 10 guts. Box-and-whisker plots on the y-axis represent the optical densities (OD) at 625 nm normalized according to the number of gut lysate samples. Note that there was no significant difference in the absorbance between the guts of *D. melanogaster* and *D. sechellia* under the HGD condition.

(B) TAG amounts in the whole bodies of *D. melanogaster* and *D. sechellia* under CD and HGD conditions. Each dot corresponds to a whole-body lysate sample prepared by squeezing 10 virgin females. The y-axis represents the amount of TAG normalized according to the amount of protein in the whole-body lysates.

(C) Circulating glucose amounts in the body fluid of *D. melanogaster* and *D. sechellia* under CD and HGD conditions. Each dot corresponds to a hemolymph sample prepared

from 30–40 adults. The y-axis represents the amount of glucose in 1 μL adult hemolymph.

*p<0.05, **p<0.001, ***p＜0.0001 (Tukey–Kramer test). n.s.: not significant.

Fig. S3. Stone formation in Malpighian tubules is not associated with the shortened lifespan of *D. sechellia* under high-glucose diet (HGD) conditions

The degree of stone formation in the Malpighian tubules of *D. melanogaster* and *D. sechellia* under control diet (CD) and HGD conditions. A five-point (from 0 to 4) scale was used to evaluate the level of stone formation in the Malpighian tubules, as previously described (van Dam et al., 2020). The y-axis represents the average score for each group divided by the number of observed Malpighian tubules. The sample numbers are presented as bars, which represent the mean ± SEM. n.s.: not significant according to the Tukey–Kramer test.

Fig. S4. Immunohistochemical observation of the gut epithelial structures of *D. melanogaster* and *D. sechellia* reared on control diet (CD) and high-glucose diet (HGD)

Gut epithelia were stained with DAPI (blue) and the following antibodies: anti-Discs large (Dlg; septate junction marker; green), anti-phosphorylated Ezrin (apical marker; pEzrin; magenta), anti-Tetraspanin-2A (Tsp2a; septate junction marker; magenta), anti-Coracle (Cora; septate junction marker; green), and anti-Mesh (septate junction marker; magenta). We focused on the R2 region for our observations. The upper and lower parts of each photograph correspond to the apical and basal sides of the gut epithelium, respectively. Scale bar: 100 μm.

Fig. S5. Impairment of gut barrier function is not associated with the shortened lifespan of *D. sechellia* under a high-glucose diet (HGD)

Gut barrier function was evaluated based on the activity of intestinal alkaline phosphatase (IAP), as previously described (Pereira et al., 2018). The y-axis represents the absorbance at 405 nm ($Absorb_{405}$), which corresponds to the amount of dephosphorylated pNPP, normalized according to the amount of protein in each sample. ***$p < 0.0001$ (Tukey–Kramer test). n.s.: not significant.

Fig. S6. Calcofluor White staining for visualization of dry yeast cell particles

(A) Calcofluor White staining of the dry yeast (dissolved in water) used for making fly food and the high-glucose diet (HGD).

(B) Calcofluor White staining of bacteria, fungi, and dietary dry yeast cell particles in the gut lumen of *Drosophila* reared on HGD or a diet without dry yeast (-Yeast). Some Calcofluor White-positive large particles still remained in the -Yeast condition in *D. sechellia* gut lumens. This observation suggests that *D. sechellia* reared on HGD enriches not only dry yeast cell particles, but also some unknown large particles that differ from dry yeast cells.

Long and short scale bars: 100 μm and 5 μm, respectively.

Fig. S7. Enteroendocrine tachykinin (Tk) levels were unchanged between *D. melanogaster* and *D. sechellia* in control diet (CD) and high-glucose diet (HGD) conditions

(A) Immunohistochemical observation of the guts of *D. melanogaster* and *D. sechellia* reared on CD and HGD. The guts were stained with anti-Tk antibody (magenta) and DAPI (blue). We focused our observations on the R2 region. Scale bar: 10 μm.

(B) Densitometric analysis of anti-Tk immunoreactivity. The y-axis represents the relative sum of anti-Tk immunostaining signals normalized by the area of the observed guts. a.u.: arbitrary unit. n.s.: not significant.

Fig. S8. Analysis of gut bacteria in *D. melanogaster* and *D. sechellia* reared on a high-glucose diet (HGD)

A colony formation assay was performed using gut lysates derived from *D. melanogaster* and *D. sechellia* reared on HGD. The data used for the graphical representation are the same as those used in Fig. 4A. The x-axis represents the five types of bacterial culture media: brain heart infusion (BHI), lysogeny broth (LB), liver infusion broth (LIB), Mannitol, and de Man, Rogosa, and Sharpe broth (MRS). The y-axis represents the colony formation units (CFU) from four plates of each bacterial culture medium (mean ± SEM). White and gray bars represent data for *D. melanogaster* and *D. sechellia*, respectively. * $p<0.05$, ** $p<0.01$, and ***$p < 0.001$ (Tukey–Kramer test). n.s.: not significant.

Fig. 1

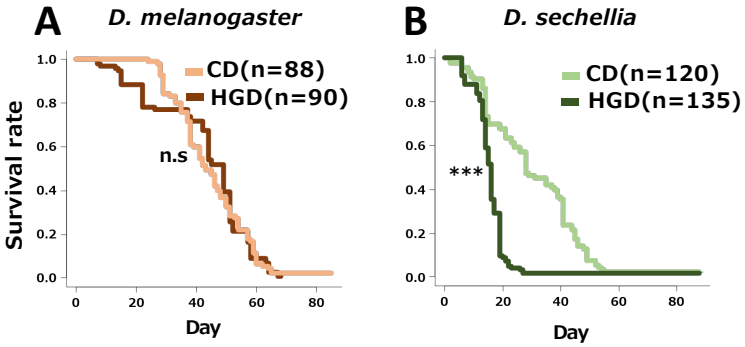
A
D. melanogaster
CD(n=88)
HGD(n=90)
n.s
Survival rate
1.0
0.8
0.6
0.4
0.2
0.0
0
20
40
60
80
Day
B
D. sechellia
CD(n=120)
HGD(n=135)
***
1.0
0.8
0.6
0.4
0.2
0.0
0
20
40
60
80
Day

Fig. 2

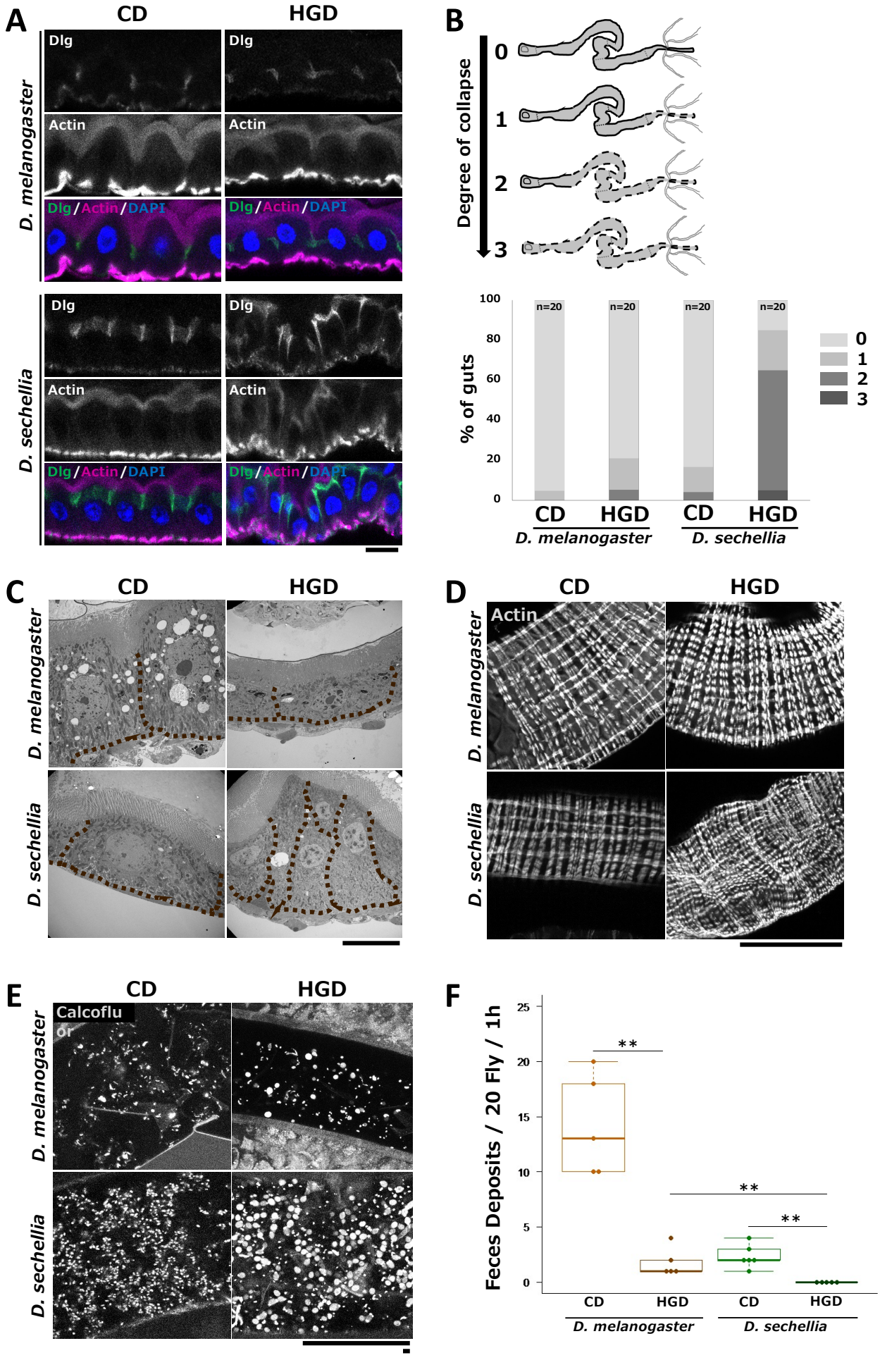
A
CD
HGD
D. melanogaster
D. sechellia
Dlg
Actin
Dlg/Actin/DAPI
B
Degree of collapse
0
1
2
3
% of guts
n=20
CD
HGD
D. melanogaster
D. sechellia
C
D
E
Calcoflu
or
F
Feces Deposits / 20 Fly / 1h
**

Fig. 3

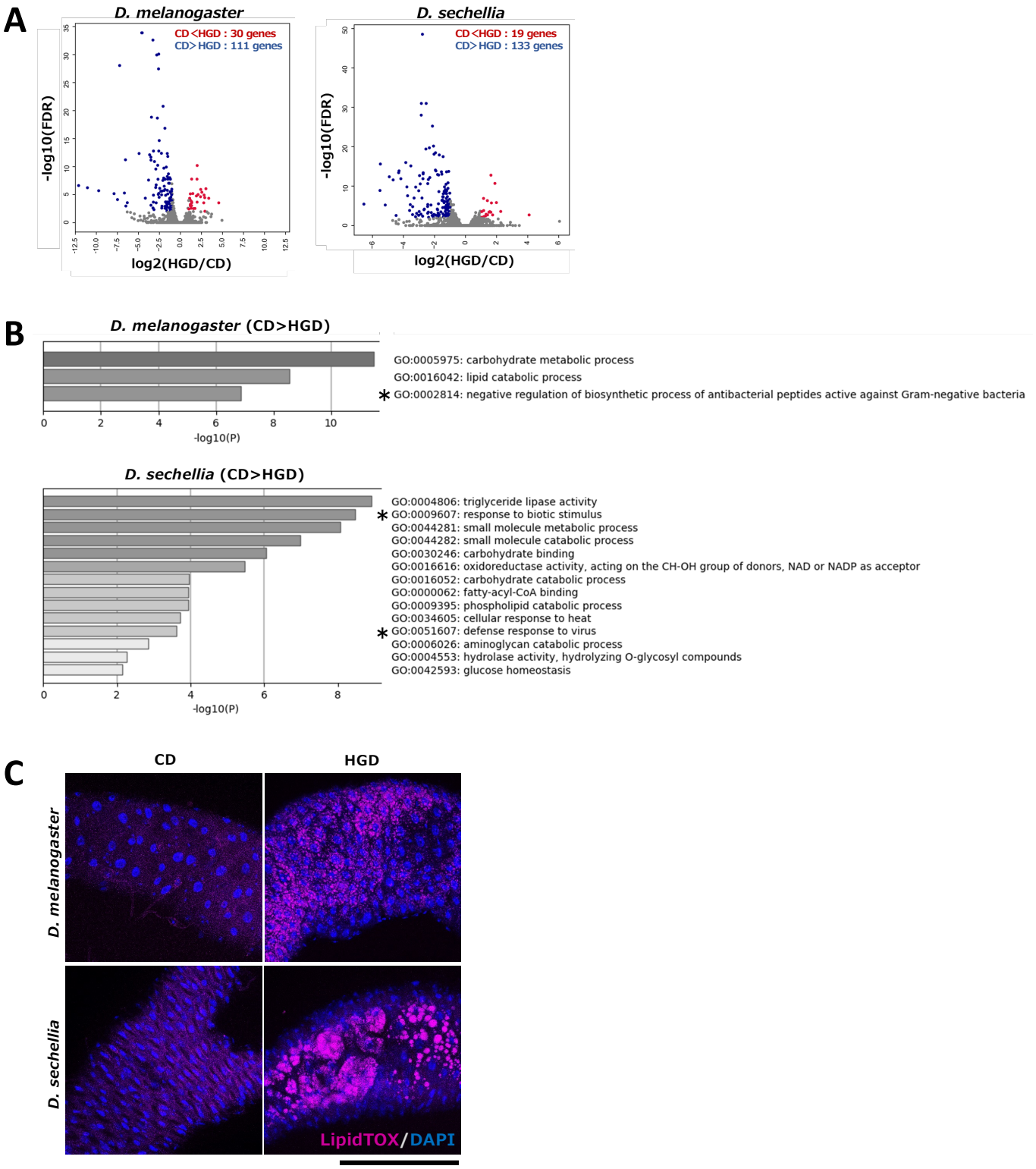
A
D. melanogaster
CD<HGD : 30 genes
CD>HGD : 111 genes
-log10(FDR)
log2(HGD/CD)
D. sechellia
CD<HGD : 19 genes
CD>HGD : 133 genes
-log10(FDR)
log2(HGD/CD)
B
D. melanogaster (CD>HGD)
-log10(P)
GO:0005975: carbohydrate metabolic process
GO:0016042: lipid catabolic process
* GO:0002814: negative regulation of biosynthetic process of antibacterial peptides active against Gram-negative bacteria
D. sechellia (CD>HGD)
-log10(P)
GO:0004806: triglyceride lipase activity
* GO:0009607: response to biotic stimulus
GO:0044281: small molecule metabolic process
GO:0044282: small molecule catabolic process
GO:0030246: carbohydrate binding
GO:0016616: oxidoreductase activity, acting on the CH-OH group of donors, NAD or NADP as acceptor
GO:0016052: carbohydrate catabolic process
GO:0000062: fatty-acyl-CoA binding
GO:0009395: phospholipid catabolic process
GO:0034605: cellular response to heat
* GO:0051607: defense response to virus
GO:0006026: aminoglycan catabolic process
GO:0004553: hydrolase activity, hydrolyzing O-glycosyl compounds
GO:0042593: glucose homeostasis
C
CD
HGD
D. melanogaster
D. sechellia
LipidTOX/DAPI

Fig. 4

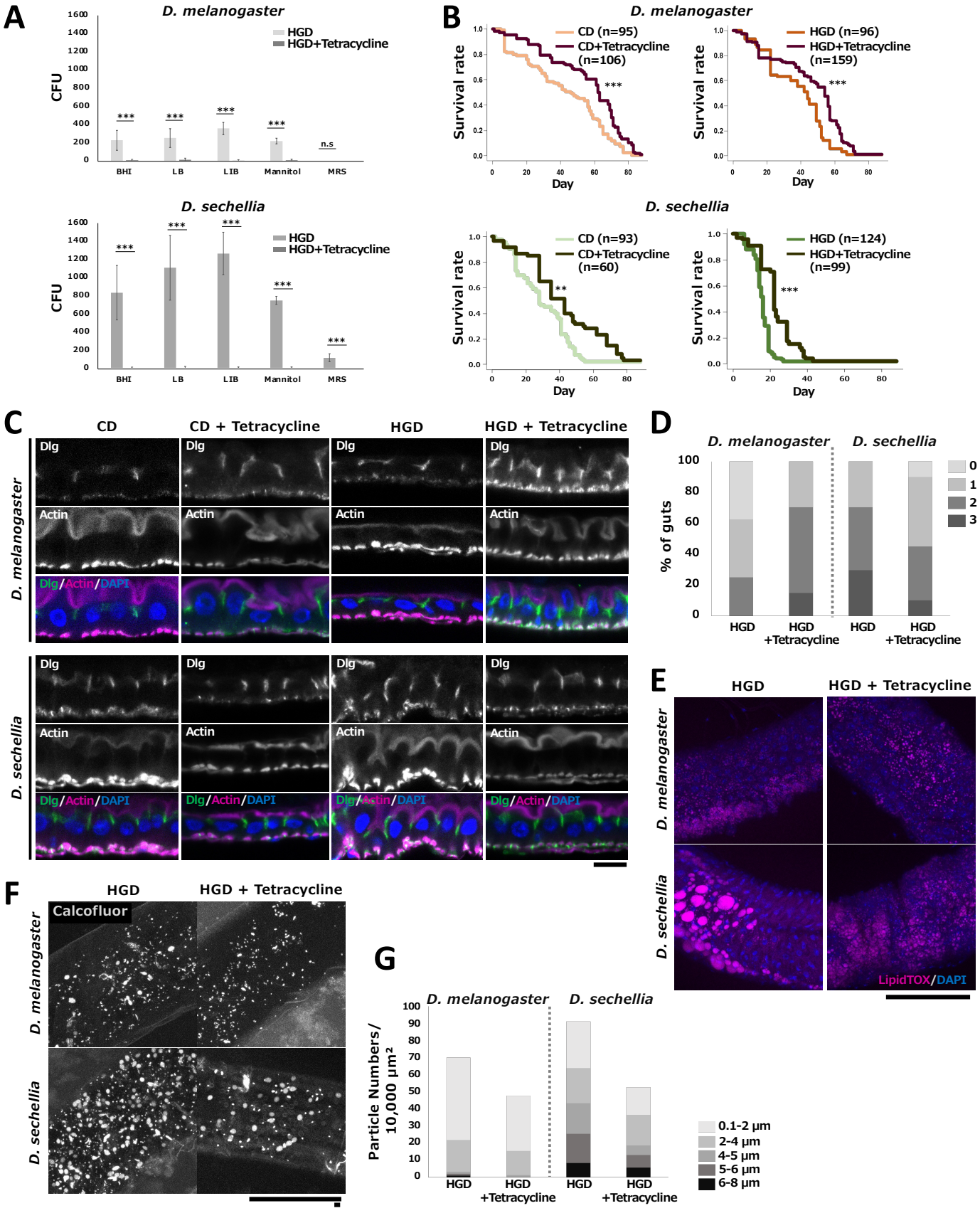
A
D. melanogaster
HGD
HGD+Tetracycline
CFU
BHI
LB
LIB
Mannitol
MRS
n.s
D. sechellia
B
D. melanogaster
CD (n=95)
CD+Tetracycline (n=106)
HGD (n=96)
HGD+Tetracycline (n=159)
Survival rate
Day
D. sechellia
CD (n=93)
CD+Tetracycline (n=60)
HGD (n=124)
HGD+Tetracycline (n=99)
C
CD
CD + Tetracycline
HGD
HGD + Tetracycline
D. melanogaster
D. sechellia
Dlg
Actin
Dlg/Actin/DAPI
D
D. melanogaster
D. sechellia
% of guts
0
1
2
3
HGD
HGD +Tetracycline
E
HGD
HGD + Tetracycline
D. melanogaster
D. sechellia
LipidTOX/DAPI
F
HGD
HGD + Tetracycline
Calcofluor
D. melanogaster
D. sechellia
G
D. melanogaster
D. sechellia
Particle Numbers/ 10,000 µm²
0.1-2 µm
2-4 µm
4-5 µm
5-6 µm
6-8 µm
HGD
HGD +Tetracycline

Fig. 5

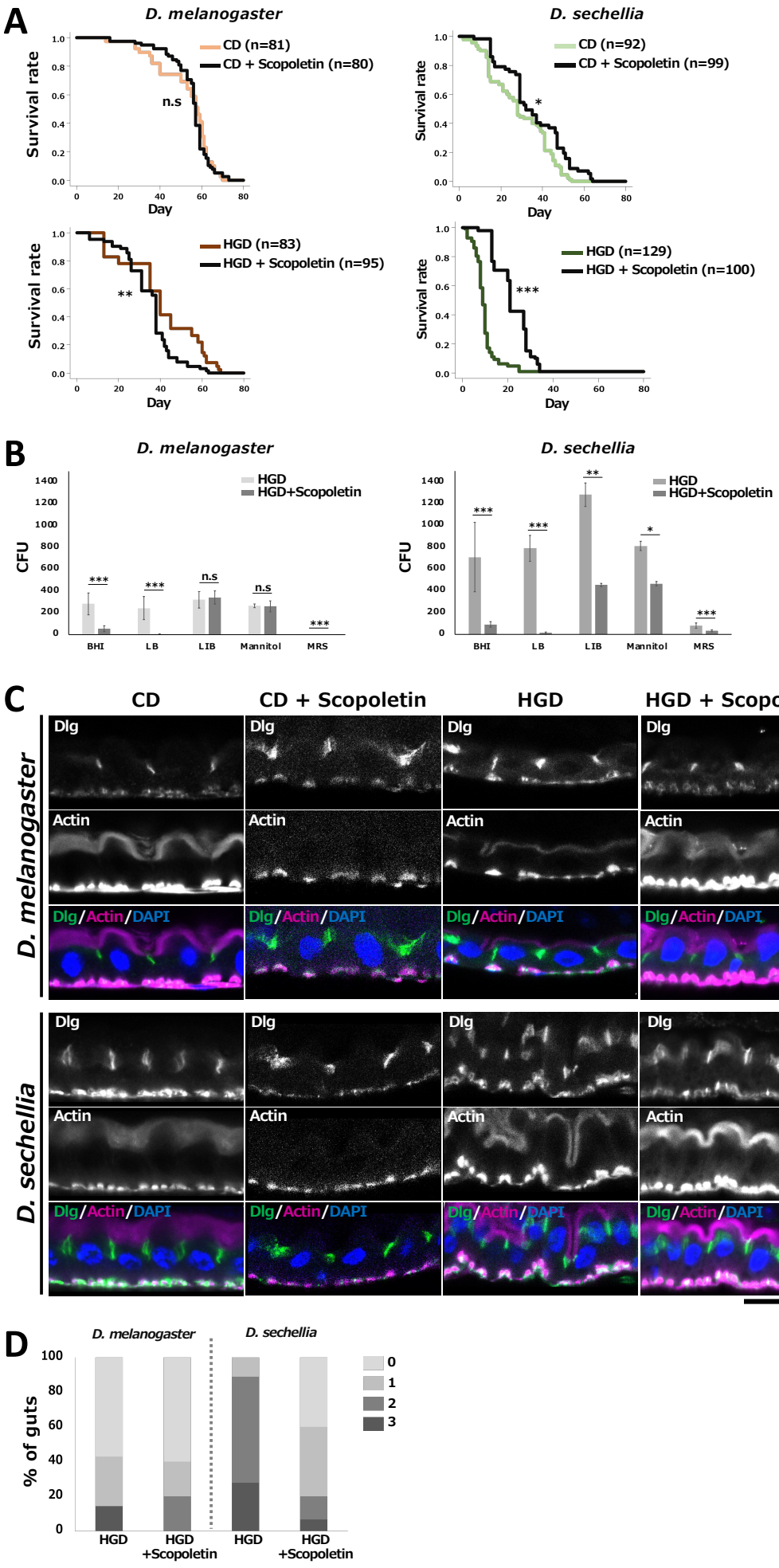
A
D. melanogaster
CD (n=81)
CD + Scopoletin (n=80)
n.s
HGD (n=83)
HGD + Scopoletin (n=95)
**
D. sechellia
CD (n=92)
CD + Scopoletin (n=99)
*
HGD (n=129)
HGD + Scopoletin (n=100)
***
Survival rate
Day
B
D. melanogaster
D. sechellia
HGD
HGD+Scopoletin
CFU
BHI
LB
LIB
Mannitol
MRS
C
CD
CD + Scopoletin
HGD
HGD + Scopoletin
D. melanogaster
D. sechellia
Dlg
Actin
Dlg/Actin/DAPI
D
% of guts
0
1
2
3
HGD
HGD +Scopoletin

Fig. 6

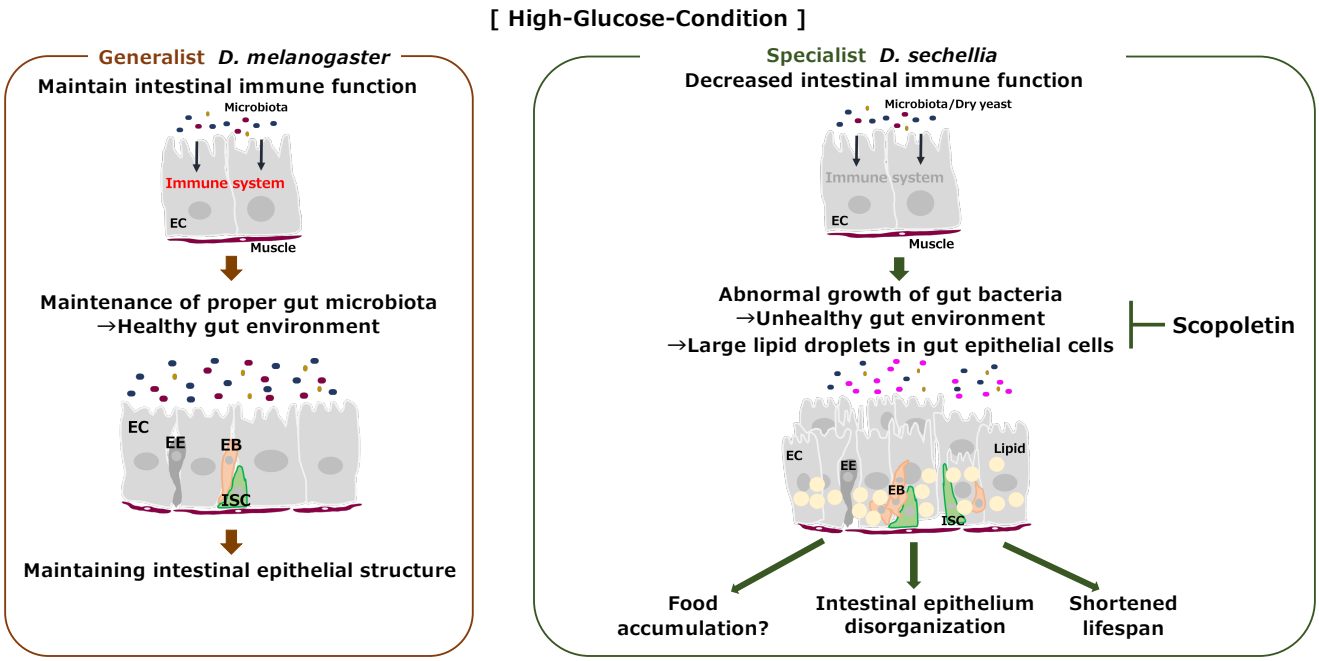
[High-Glucose-Condition]
Generalist D. melanogaster
Maintain intestinal immune function
Microbiota
Immune system
EC
Muscle
Maintenance of proper gut microbiota
→Healthy gut environment
EC
EE
EB
ISC
Maintaining intestinal epithelial structure
Specialist D. sechellia
Decreased intestinal immune function
Microbiota/Dry yeast
Immune system
EC
Muscle
Abnormal growth of gut bacteria
→Unhealthy gut environment
→Large lipid droplets in gut epithelial cells
Scopoletin
EC
EE
EB
ISC
Lipid
Food accumulation?
Intestinal epithelium disorganization
Shortened lifespan

Supplementary Fig. S1

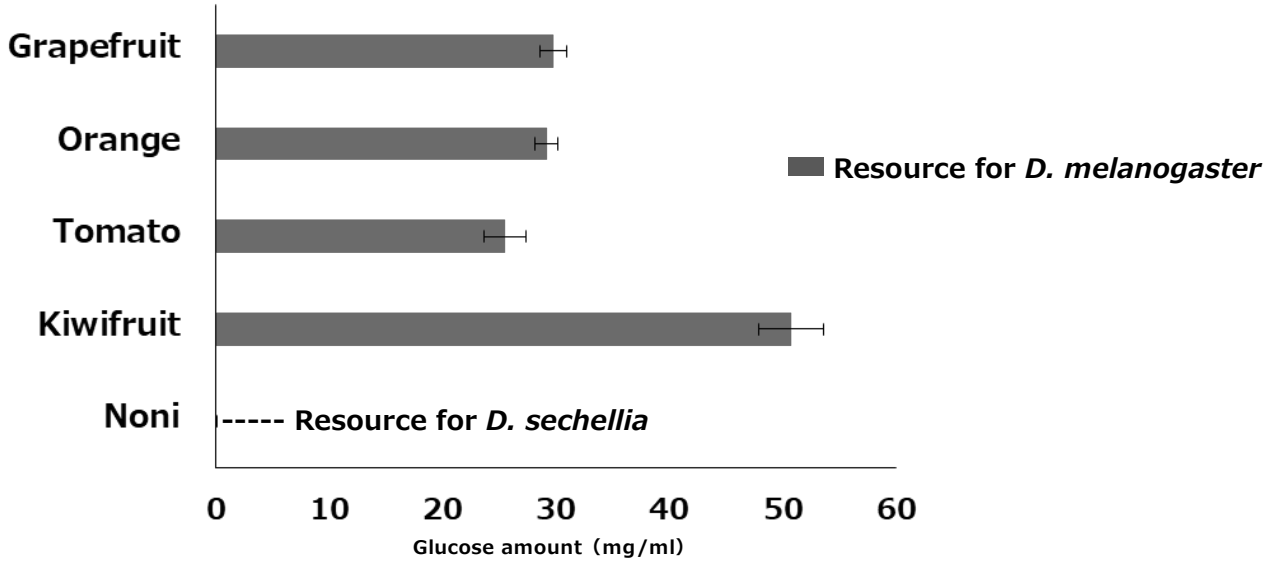

Supplementary Fig. S2

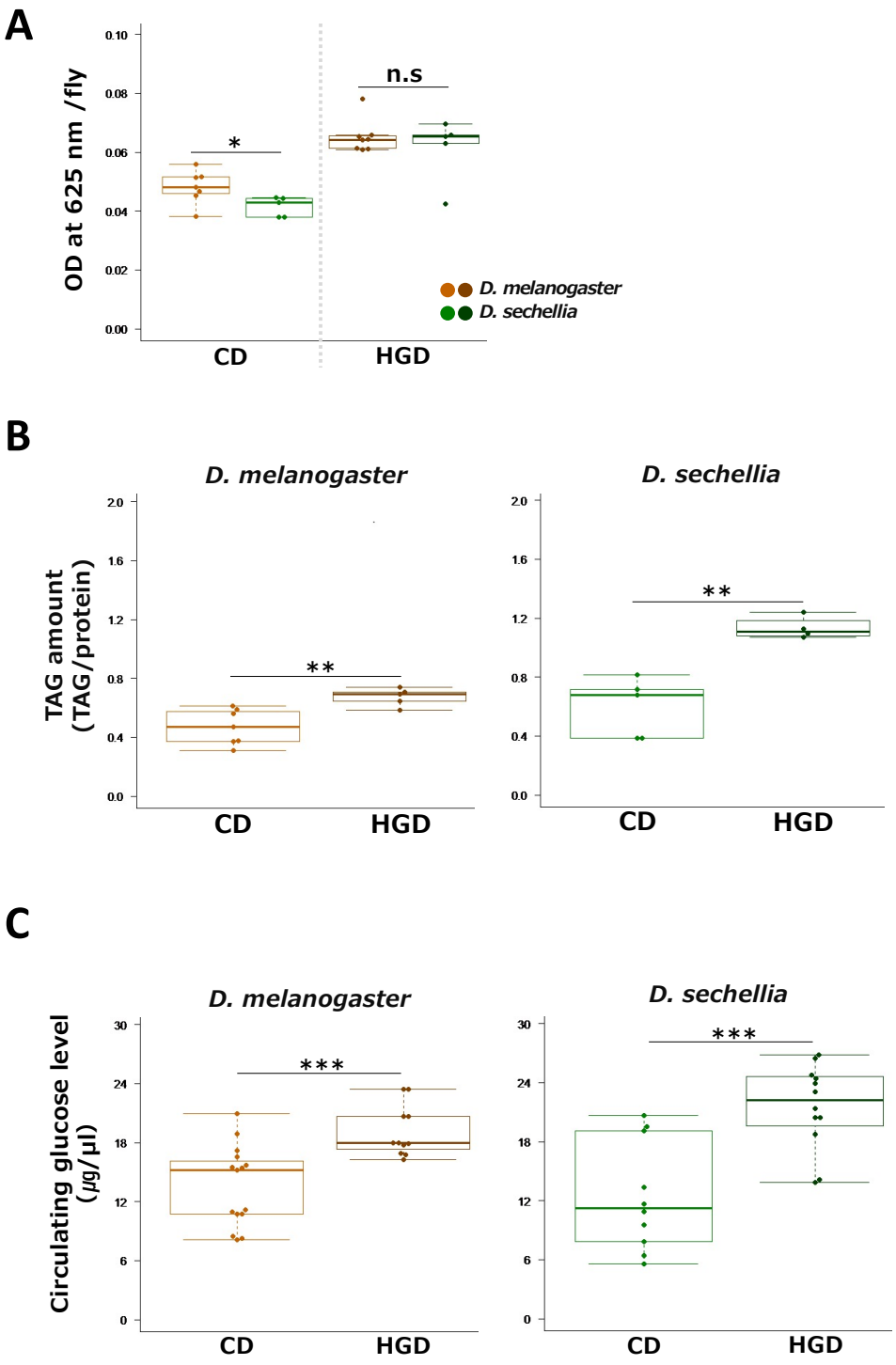

Supplementary Fig. S3

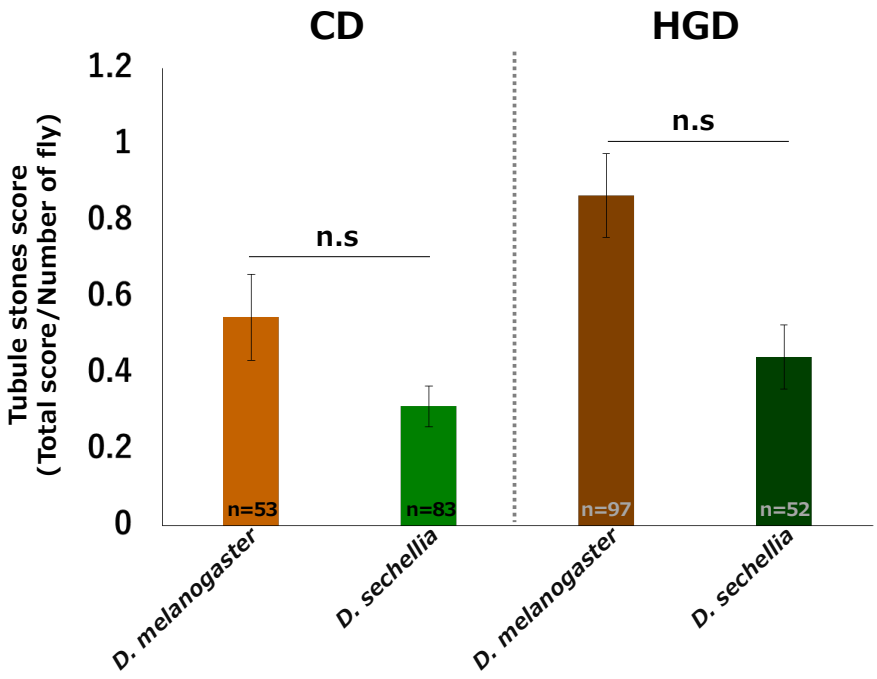

Supplementary Fig. S4

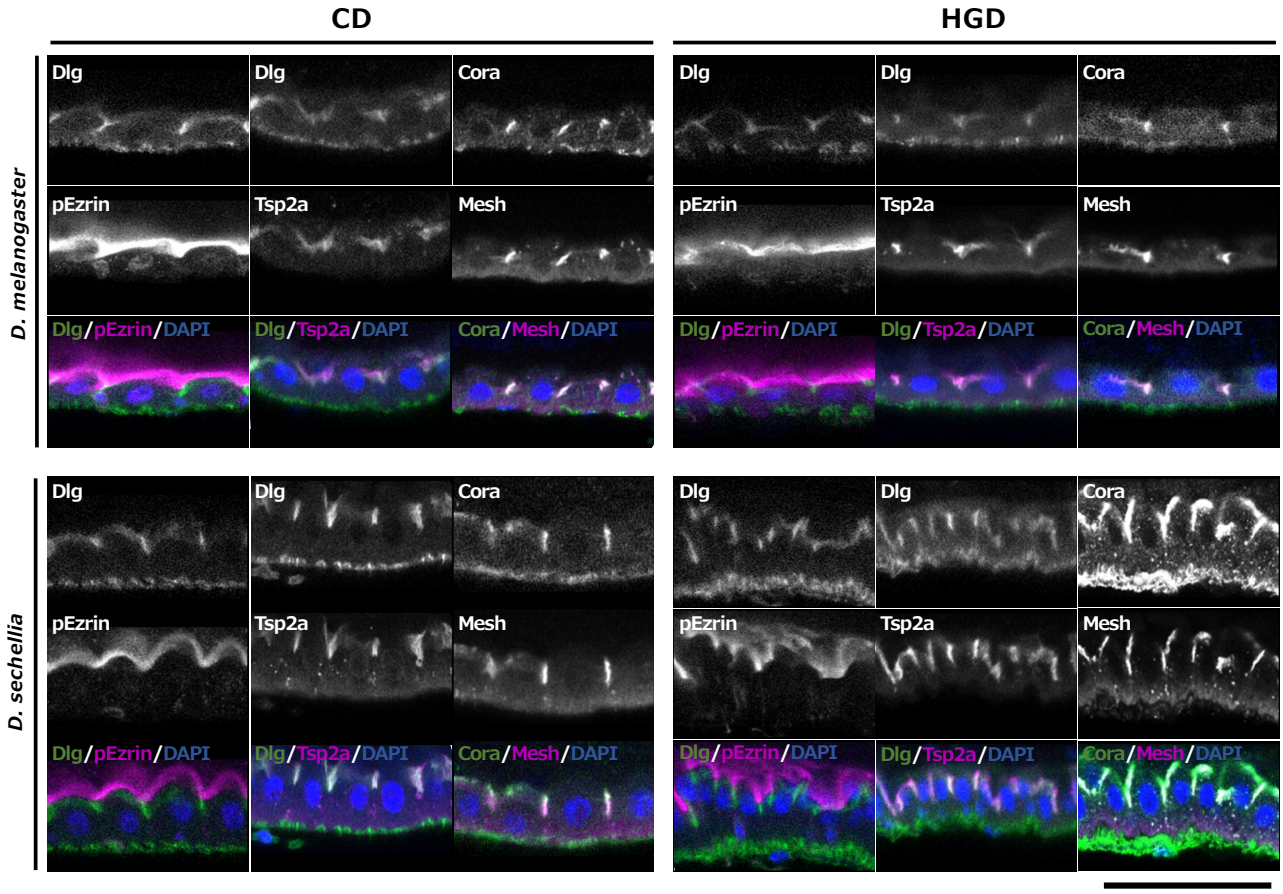

Supplementary Fig. S5

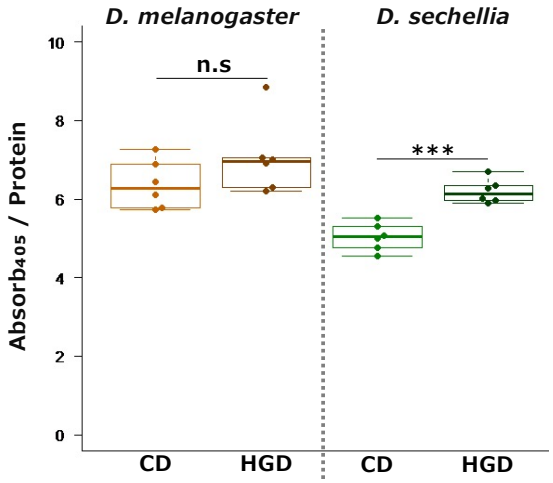

Supplementary Fig. S6

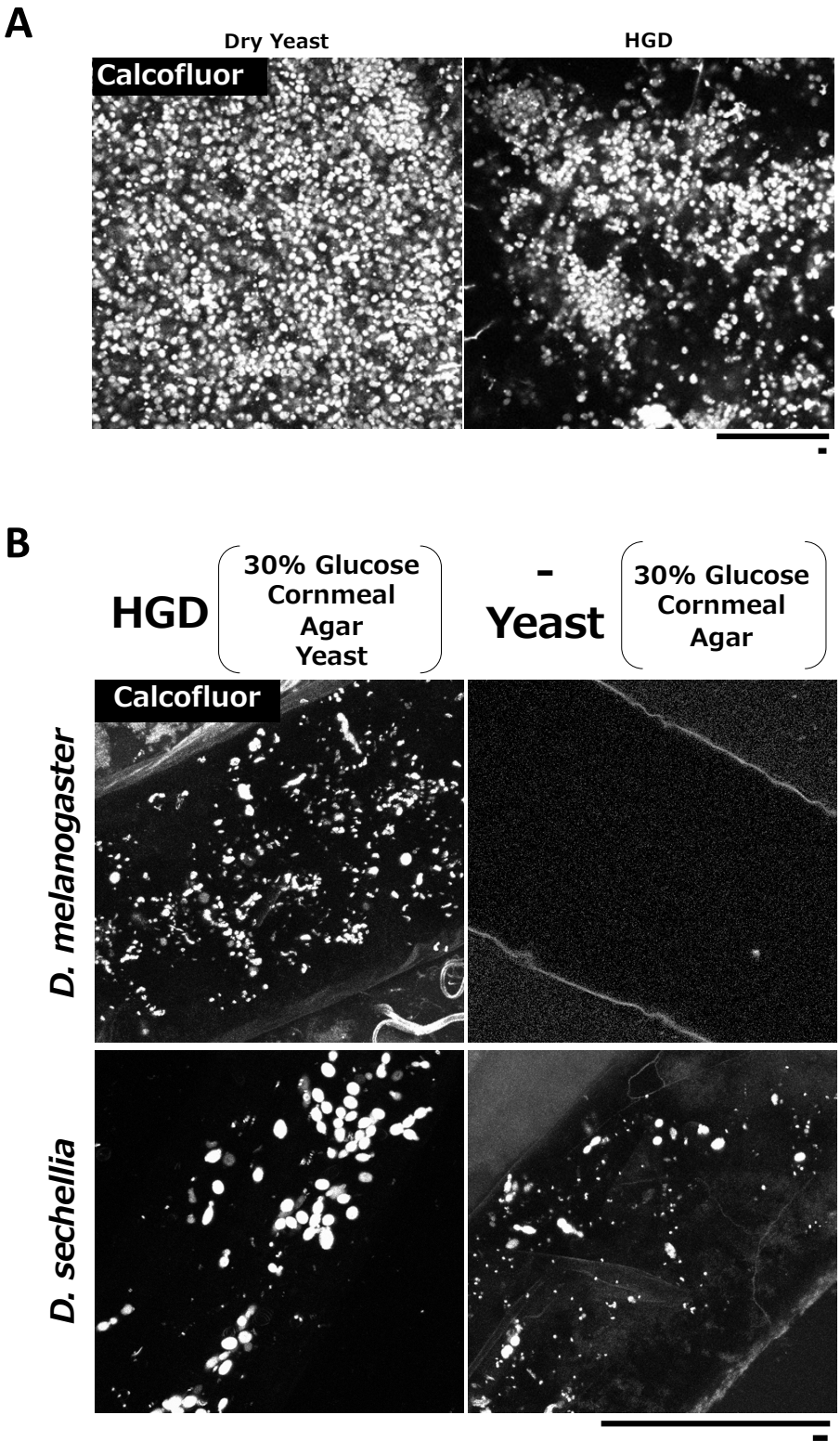

Supplementary Fig. S7

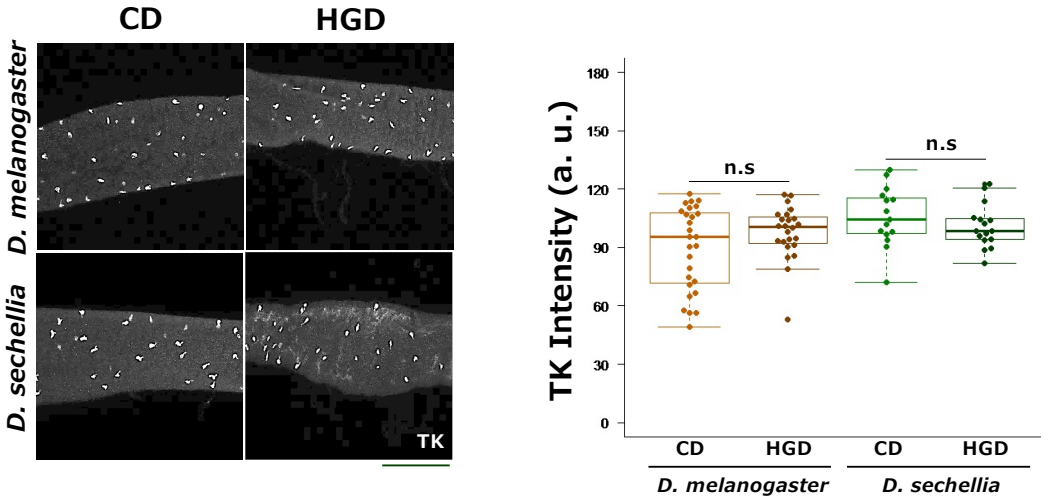

Supplementary Fig. S8